Graduate School Form 30
(Revised 08/14)

PURDUE UNIVERSITY
GRADUATE SCHOOL
Thesis/Dissertation Acceptance

This is to certify that the thesis/dissertation prepared

By Omar Nezamuddin

Entitled
POWER ELECTRONICS SOLUTIONS FOR UNINTERRUPTED POWER SUPPLY AND GRID-TIE INVERTERS

For the degree of Master of Science in Electrical and Computer Engineering

Is approved by the final examining committee:

Euzeli dos Santos

Maher E. Rizkalla

Steven Rovnyak

To the best of my knowledge and as understood by the student in the Thesis/Dissertation Agreement, Publication Delay, and Certification/Disclaimer (Graduate School Form 32), this thesis/dissertation adheres to the provisions of Purdue University's "Policy on Integrity in Research" and the use of copyrighted material.

Euzeli dos Santos

Approved by Major Professor(s): _____

_____

Approved by: Brian King 11/21/2014

Head of the Department Graduate Program Date

POWER ELECTRONICS SOLUTIONS FOR UNINTERRUPTED POWER SUPPLY AND GRID-TIE INVERTERS

A Thesis

Submitted to the Faculty

of

Purdue University

by

Omar N. Nezamuddin

In Partial Fulfillment of the

Requirements for the Degree

of

Master of Science in Electrical and Computer Engineering

December 2014

Purdue University

Indianapolis, Indiana

For the best parents anyone could ask for:
Dr. Nabeel Nezamuddin and Dr. Farida Mirza.

ACKNOWLEDGMENTS

First, I would like to take this opportunity to thank my parents for all their love, encouragement, and never ending support for everything. To them I owe everything and could never return the favor. I dedicate all my work to you, Dad & Mom. Now and always, Thank You. I also thank my awesome siblings and wife, Sarah, Ibraheem, Nora, and Cansu, for all their continued support of my education, and continuously providing me with the help I need. I could have never done this without all your support.

I would also like to thank the whole ECE department, with special thanks to the following: To Dr. Euzeli dos Santos Jr, for his continuous support, the great opportunities he has opened for me, and for supporting and guiding me in my educational endeavor. To Dr. Maher Rizkalla, for all his support, his constant belief in me, and for encouraging me to pursue my masters degree. To Dr. Steven Rovnyak, for all his support and for involving me in great opportunities with the department. To Dr. Brian King for his support of my pursuit of higher education, and always being there when needed. To Sherrie Tucker, space is too limited to list everything she has done and all the help she's provided me throughout my career, but I will mention this - if it was not for her, I would have missed so many deadlines. I truly thank her for all the support and constant guidance throughout my time as a student.

Additionally, a thank you to Jigar, of Sunrise Electronics Inc, for his support in all our projects. And last but not least, I would like to thank His Majesty King Abdullah Bin Abdulaziz Al-Saud, and the Government of Saudi Arabia, for providing me the opportunity to conduct my studies through their generous support.

TABLE OF CONTENTS

Page

LIST OF TABLES

LIST OF FIGURES

ABSTRACT

Nezamuddin, Omar N. MSECE, Purdue University, December 2014. Power Electronics Solutions for Uninterrupted Power Supply and Grid-Tie Inverters. Major Professor: Euzeli dos Santos Jr.

This thesis proposes two new topologies for Uninterrupted Power Supply (UPS), and a grid-tie microinverter. The first topic will discuss an on-line transformerless UPS system based on the integrated power electronics converters that is able to control the input power factor, charge the battery, and guarantee backup operation of the system. The main advantages of the proposed UPS are active power factor correction (PFC) without the need of a complex control scheme, and integrated functions of the battery charger circuit and PFC with only three power switches. Operation modes of the system and the PWM strategy is presented in detail. The second topic discussed is of a proposed circuitry for a single-phase back-to-back converter for UPS applications. The main advantages of this topology is higher number of levels at the rectifier side, less number of power switches, and no need for a boost inductor at the input side of the converter. The last topic discussed is of a proposed patent pending microinverter. This topic was a project funded by the National Science Foundation, and its aim was to help commercialize the research. This project proposes a solution for a solar inverter called Delta Microinverter that allows easier and faster installation as well as power conversion with higher efficiency. Delta Microinverters innovation is found in its patent-pending shape and in its patent-pending circuitry, i.e., electronics mounted inside of the Delta Microinverter. The Delta Microinverters shape has a housing configured for rapid mounting using a single fastener and its power electronics configuration offers an optimized relationship between the number of levels and number of power switches.

1. INTRODUCTION

The objective of this thesis is to present new power electronics solutions for uninterrupted power supply (UPS) systems and grid-tie inverters. This thesis is divided into five chapters. The first chapter will introduce a comprehensive review of power electronics applied to UPS and grid-tie solar inverters. The second chapter proposes a solution for UPS systems which is based on a new transformerless integrated power converter. Emphasis will be on power factor control (PFC), model, PWM strategy, and battery voltage management. Chapter 3 deals with an optimized circuitry for a single-phase back-to-back converter, with focus on the principles of operation, PWM strategy, and control. Chapter 4 deals with a patent-pending circuitry and shape (physical) of a grid-tie microinverter. The circuity will be discussed in two sections, and the shape in another. Chapters 2, 3, and 4 present simulated or experimental results to validate the proposed topologies. The final chapter will be a summery that goes over the presented chapters.

1.1 UPS systems

UPS is an electrical device with a main purpose of supplying emergency power when there are blackouts or brownouts. Such systems are often used for the protection of devices such as computers, telecommunication equipment, medical equipment, and many other electrical devices where power loss could cause serious problems or injuries [1–3]. UPS units range in size [4–6], they could power up anything from 200 VA to 46 MVA.

Among the three major types of UPS (off-line, line-interactive, and on-line [24]), the on-line one offers some advantages such as protection of critical load from either voltage or frequency fluctuation with the utility power line. Such an on-line UPS can

also preserve critical loads from spikes, sags and grid load voltage harmonics. Considering the power electronics point of view, an on-line UPS presents three conversion units as presented in Fig. 1.1, they are: rectifier, inverter and dc-dc bidirectional converter. During the normal operation of the on-line UPS, the energy from the grid is employed to supply the load and also charge the battery. If the battery is fully charged, the energy flows strait from the grid to the load through rectifier and inverter blocks. In the case of grid outage, the system should be able to send the energy stored in the battery to the load.

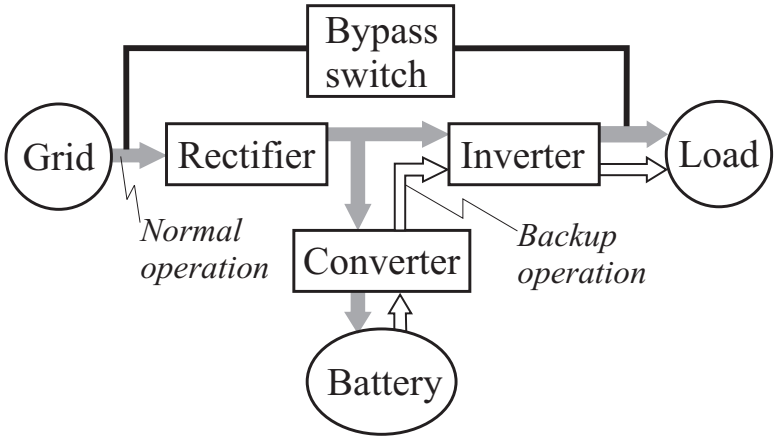

Fig. 1.1. Simplified schematic of an on-line UPS.

A line-interactive UPS with reduced cost was proposed by [25] offering the characteristics of an on-line UPS. Such an UPS is based on the combination of two full-bridge VSI converters connected in series with the input and the second one in parallel with the load. On the other hand, [26], [27] presented a DSP-controlled on-line UPS with transformerless for single-phase applications with balanced charging and discharging control capability. In [28] was proposed an UPS system with reactive power compensation. Another example of on-line UPS with power factor correction and electrical isolation is proposed by [29], [30]. The power factor correction based on the boost converter is the most popular technique to achieve unity power factor [28], [30], [31]

in UPS and others power electronics-based equipment. The implementation and design of a PIC microcontrolled on-line UPS is shown in [38], power factor correction is also implemented in the design using a switch mode power supply module. Another example showing power factor correction based on an intrinsic boost converter was discussed in [43].

Another topology with a feedback control system for regulating the battery voltage supplying the inverter was discussed in [39]. There are plenty of different topologies for charging the battery of the UPS system, such as using photovoltaic panels as discussed in [41]. Other topologies, like [42], show the use of fuel cell instead of batteries for backup operations. Topologies like this have plenty of advantages such as higher power density, efficiency, and less maintenance costs. There has also been some research regarding early detection of faults for on-line batteries shown in [40].

Single-phase to single-phase back-to-back converter is the center piece device for different industrial electric apparatus, such as active power filter [24], motor drive systems [25], and specially for (UPS) systems like [36] and [37].

A conventional back-to-back converter used in an UPS system can be employed with either eight power switches, as presented in Fig. 1.2(a), or with six power switches, as presented in Fig. 1.2(b). Notice that the six power switch converter employs a shared leg between both input and output sides of the converter [34]. This topology is especially interesting for applications such as UPS due to optimization brought up by a synchronization technique [33].

1.2 Grid-Tie Inverters

Grid-tie inverters are essentially inverters that change electricity from direct current (DC) to alternating current (AC) and are typically used with solar panels [7–13]. Some of the main advantages of the grid-tie system compared to others (off-grid and grid-tie with batteries) is lower cost for initial setup, lower maintenance in the long run, less complexity, and higher efficiency [55]. One of the most important features of

the grid-tie inverter is its ability to synchronize the inverted power obtained from the DC source with the utility grid. In fact, these devices should align the voltage and current in phase with the utility grid within 1 degree. Fig. 1.3 [56] shows a simple diagram of how a Grid-tie inverter works [54], which is usually associated with either solar panels or wind turbines. These devices can be used for residential or commercial applications.

Grid-tie inverters are associated with either solar or wind energy [18, 19]. There are three types of devices used as solar grid-tie inverters: Microinverters, string inverters, and central inverters.

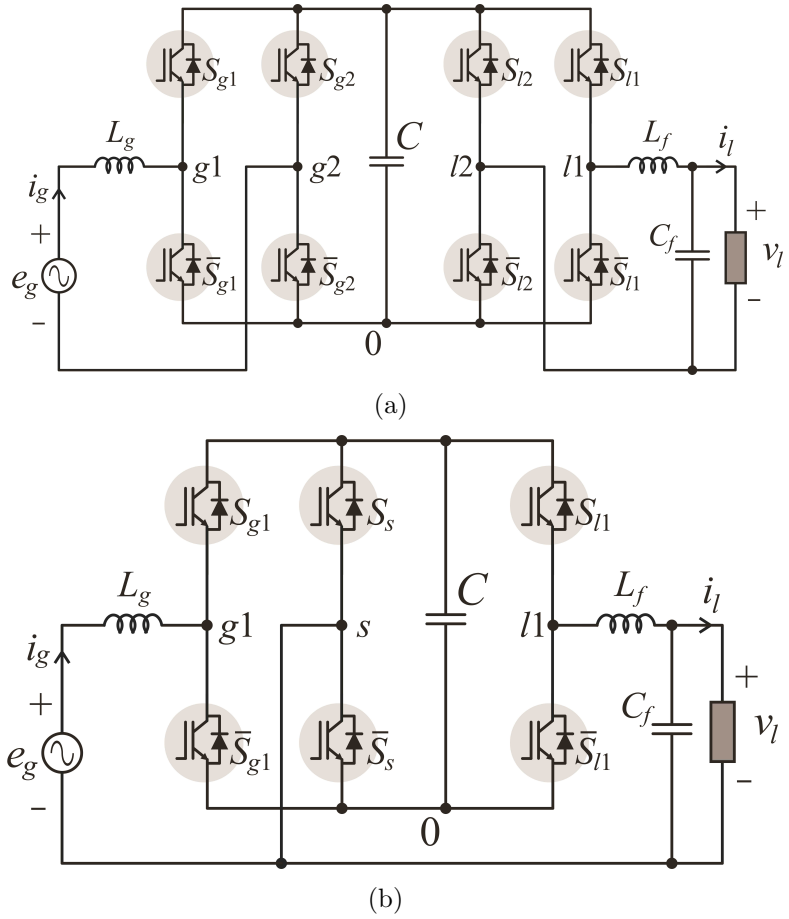

Fig. 1.2. (a) Conventional single-phase converter with eight power switches. (b) Shared-leg topology with six power switches.

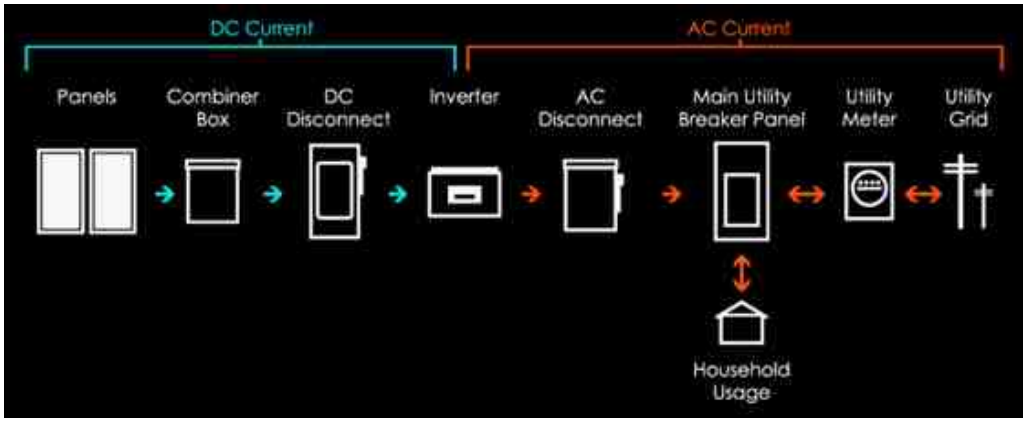

Fig. 1.3. Grid-Tie inverter block diagram.

Microinverters are usually attached to the back of a single solar module, and then combined with the output of other microinverters connected in parallel [14–17]. The string and central inverters work in a different manner, such that solar modules are connected together in series then fed into one of the inverters [22, 23]. The issue with such systems is when shading or complete failure occurs to one of the solar modules, the whole system is affected since they are connected together in series. Microinverters and string inverters are usually associated with residential applications, whereas central inverters (and sometimes string inverters) are associated with commercial systems.

2. UPS BASED ON A NEW TRANSFORMERLESS INTEGRATED POWER CONVERTER

A new transformerless on-line UPS system is proposed, which is based on the integrated power electronics converters able to control the input power factor, charge the battery, and guarantee backup operation in the case of utility power outage. Also, a controlled load voltage is obtained with the proposed circuit. The system is presented in Fig. 2.1(b), where LPF stands for Low-Pass-Filter. The input power factor control is based on the principle presented in [32], which improves the input power factor and input current waveform without any feedback control strategy. Fig. 2.1(a) shows a transformerless on-line UPS constituted by a conventional set of power converters, i.e., controlled rectifier, bidirectional dc-dc converter interfacing the battery and dc-link voltage, and an inverter. Such a converter is able to control input power factor, guarantee battery management and regulated load voltage. However, it employs ten power switches.

Comparing both Figs. 2.1(a) and 2.1(b), there is a reduction of 30% on the number of power switches employed by the proposed converter. Notice that, the static bypass switch designed to connect the load to the grid voltage in the case of power conditioner failure [see Fig. 1.1], is not presented in Figs. 2.1(a) and 2.1(b). Selected steady-state and transient outcomes are presented to validate the operation of the proposed converter as an UPS system.

2.1 Power Factor Control

The input converter side consists of a diode bridge (D_1, D_2, D_3, and D_4), two small capacitors(C_1 and C_2), two inductors (L_1 and L_2) and three power switches (S_{1a}, S_{1b}, and S_{1c}) constituting a three-switch leg. To guarantee power factor equal

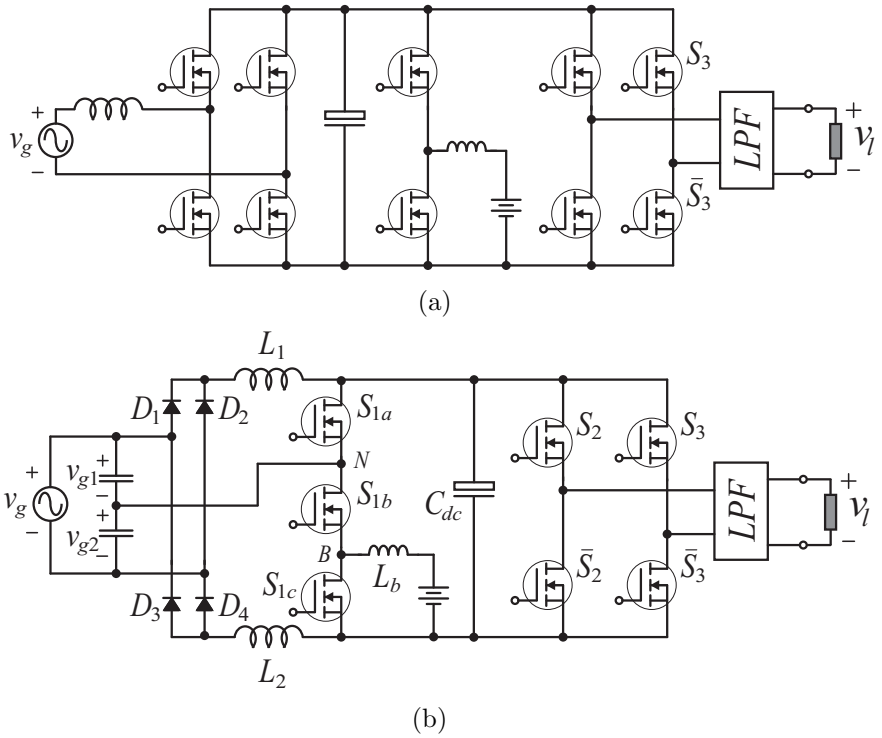

Fig. 2.1. (a) Conventional UPS power converter. (b) Proposed UPS with integrated power converter.

to one as well as a sinusoidal grid current (i_g), the voltage v_{N0} (between the point N and 0) must have a constant duty cycle equal to 0.5 at a frequency much higher than the grid frequency.

Eight modes of operation are presented in Fig. 2.2. While Figs. 2.2 (a)-(d) show the modes of operation for the positive half cycle of the grid voltage, Figs. 2.2(e)-(h) show those modes for the positive half cycle of v_g. In mode 1 [Fig. 2.2(a)] the switch S_{1a} is switched ON which allows the current flowing through C_1-D_1-L_1-S_{1a}. Energy stores up in L_1, while a discharge current of the dc-link capacitor C_{dc} flows through the output converter side. In mode 2, S_{1a} is switched OFF while S_{1b} along with S_{1c} are switched ON at the same time. Then, the stored energy of L_1 is released to the output converter side and C_{dc} via S_{1b}-S_{1c}-C_1-D_1, while L_2 stores energy by a current though C_2-S_{1b}-S_{1c}-D_4. After all energy in L_1 is released, mode 3 starts, similarly to

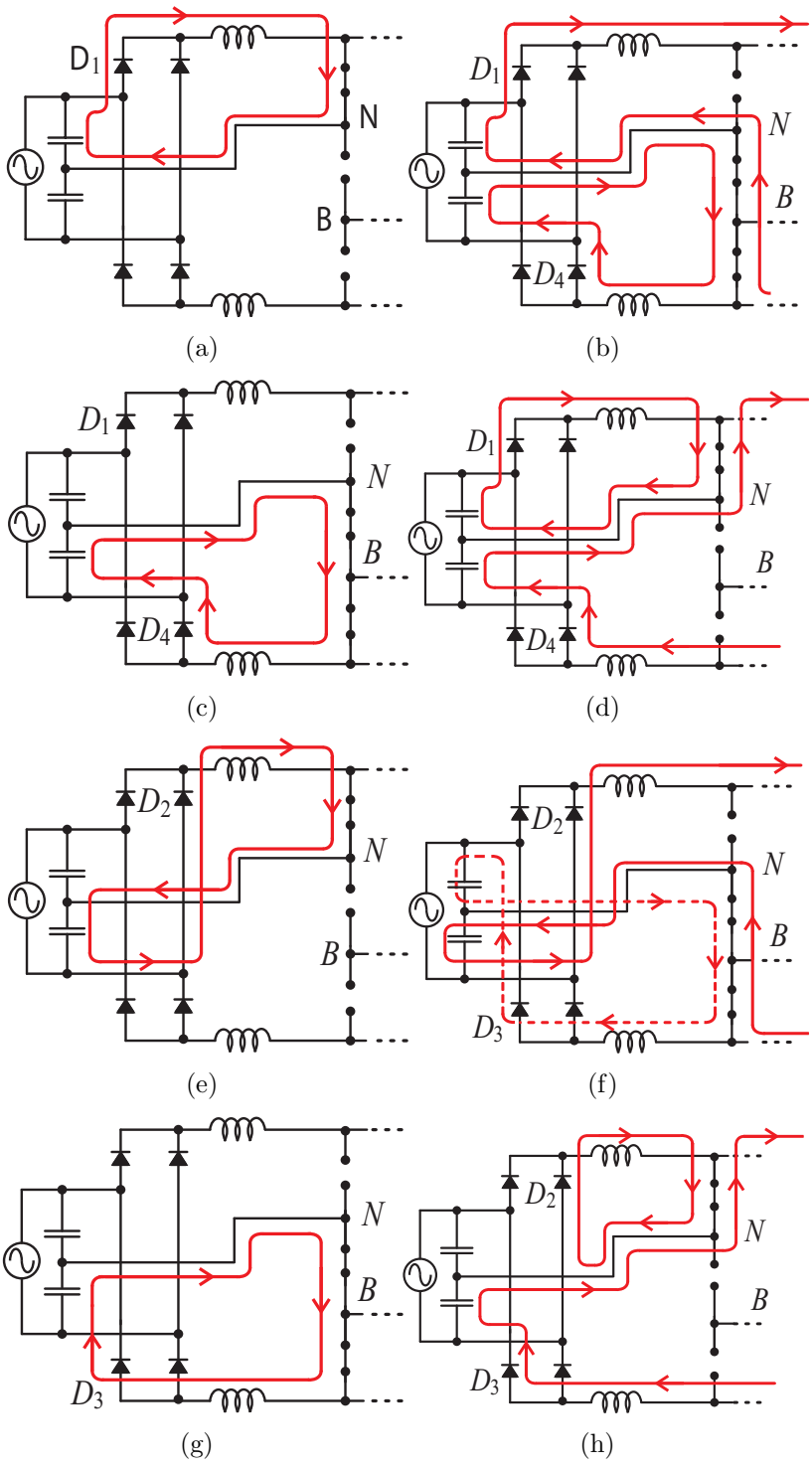

Fig. 2.2. Modes of operation for the input side of the proposed converter: (a) mode 1, (b) mode 2, (c) mode 3, (d) mode 4, (e) mode 5, (f) mode 6, (g) mode 7, and (h) mode 8.

mode 1, but with the parts related to the bottom side of the converter (L_2). So it is for Mode 4. The average value of the grid current can be written as:

$$i_g = \frac{e_g T_s}{16L} \frac{1}{(1 - e_g/2V_{dc})} \tag{2.1}$$

If $2V_{dc} > v_g$, then i_g is approximately sinusoidal.

The grid current can be written as a function of the diode currents, as below:

$$i_g = i_{D1} - i_{D3} \tag{2.2}$$

$$i_g = i_{D4} - i_{D2} \tag{2.3}$$

The inductor currents, in return, are given by:

$$i_{L1} \rightarrow i_{D1} \text{ or } i_{D3} \tag{2.4}$$

$$i_{L2} \rightarrow i_{D3} \text{ or } i_{D4} \tag{2.5}$$

Then, it is obtained from (2.2) and (2.3) that:

$$2i_g = i_{D1} - i_{D2} - i_{D3} + i_{D4} \tag{2.6}$$

For the positive and negative half cycle of the grid voltage, the grid current will be given respectively by :

$$i_g = (i_{L1} + i_{L2})/2 \tag{2.7}$$

$$i_g = -(i_{L1} + i_{L2})/2 \tag{2.8}$$

2.2 Model and PWM stratigies

The three-switch leg plays an important role for the operation of the proposed on-line UPS. This leg is composed of the power switches S_{1a}, S_{1b}, and S_{1c}. A binary

variable is associated with each switch, (i.e., $S_{1x} = 1$ is used when the switch is closed, and $S_{1x} = 0$ when the power switch is open, with $x = a$, b, c). Notice that, as observed on the conventional converter (with two switches per leg), the switches in the three-switch leg cannot be turned on simultaneously, which will avoid a short-circuit through dc-link capacitor. In this way, eight possible switching states could be obtained for this leg, since there are three switches with two switching states each ($S_{1x} = 1$ and $S_{1x} = 0$). Many of these switching states are prohibited, because of either a short-circuit or one of the unwanted switching states. For instance, when it is trying to generate either lower voltage at point N than that at point B or higher voltage at point B than that at point N [see Fig. 1(c)]. Table 2.1 shows all possible states with the indication of no-prohibited states, which are highlighted in this table.

From Table 2.1 it is possible to write equations for the voltages V_{N0} and v_{B0} as a function of the three-switch leg and the dc-link voltage V_{dc} as follows:

$$v_{N0} = [S_{1a}(1 - S_{1b}S_{1c})]\, V_{dc} \tag{2.9}$$

$$v_{B0} = [S_{1a}S_{1b}(1 - S_{1c})]\, V_{dc} \tag{2.10}$$

The model presented in (2.9) and (2.10) indicates that the voltages v_{N0} and v_{B0} is a function of the switches states. Then, the PWM signals will be generated to satisfy the converter's requirement for the power factor correction at the grid side and energy management of the battery. Fig. 2.3(a) shows an analog PWM solution employed for the three switch leg. As described in Section 2.1.1, for the correct operation of the circuit, the voltage v_{N0} must be modulated with a constant duty cycle equal to 0.5. Fig. 2.3(b) (top) shows a comparison between the reference voltage (V_N^*) and carrier signal (v_t) needed to keep a 50% duty cycle. Due to the requirement of $v_{N0} > v_{B0}$, the maximum duty cycle for the switch S_{1c} will be also 50%, but as indicated in Fig. 2.3(b) (bottom) it is possible to change V_{bat}^* to guarantee battery management.

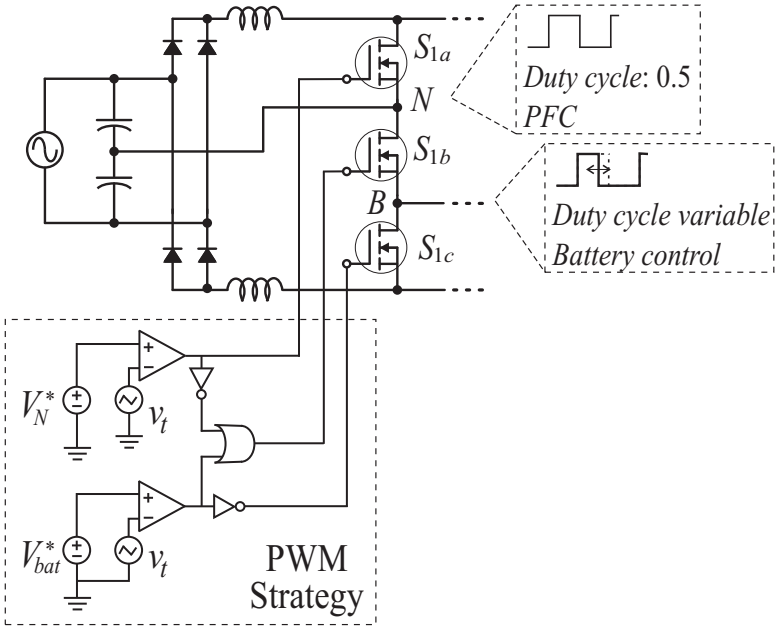

(a)

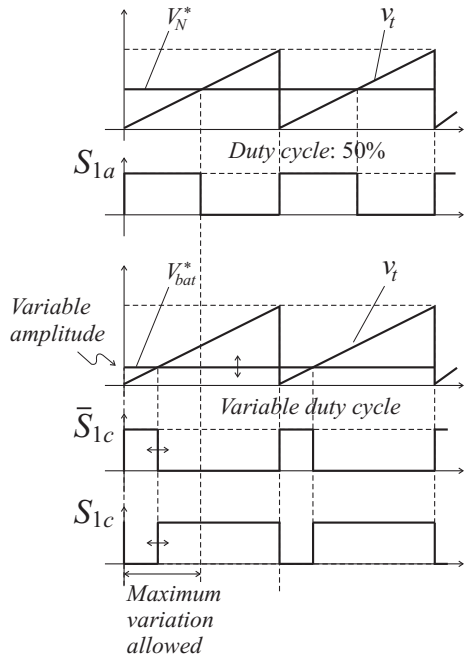

(b)

Fig. 2.3. (a) PWM strategy. (b) Main PWM signals.

Table 2.1.
Indication of prohibited switching states of three-switch leg.

States	S_{1a}	S_{1b}	S_{1c}	Prohibited States
1	0	0	0	Yes
2	0	0	1	Yes
3	0	1	0	Yes
4	0	1	1	No
5	1	0	0	Yes
6	1	0	1	No
7	1	1	0	No
8	1	1	1	Yes

2.3 Battery Voltage Management

Considering the battery's point of view, there are two operation modes depending on the utility power conditions. For a normal operation, i.e., with a rated voltage available at the grid side, the battery must be charged until reaching the stand by mode. On the other hand, when a disruption is detected by the control system, the battery must furnish the energy demanded by the load. In both cases, normal and abnormal grid conditions, the energy is processed by the dc-ac converter, which guarantees a desirable load voltage free of sags, swells, and variations of frequency. Fig. 2.4 shows the schematic for the battery energy management system. The grid conditions is detected by measuring v_g, for the normal condition the relay must be turned on and the voltage V^*_{bat} is generated to charge the battery, which is obtained through I_{bat}.

On the other hand, for the abnormal grid voltage,the relay must be turned off and the switch S_{1a} must be turned on. In this case the V^*_{bat} is employed to keep the dc-link voltage constant V_{dc}. R_1 and R_2 is used as a voltage divider.

Fig. 2.5(a) shows the control implemented to charge the battery. $V^*_{charger}$ is the voltage needed to charger the battery, its value will depend on the number and association of batteries employed on the UPS. C is a PI controller. Fig. 2.5(b), in

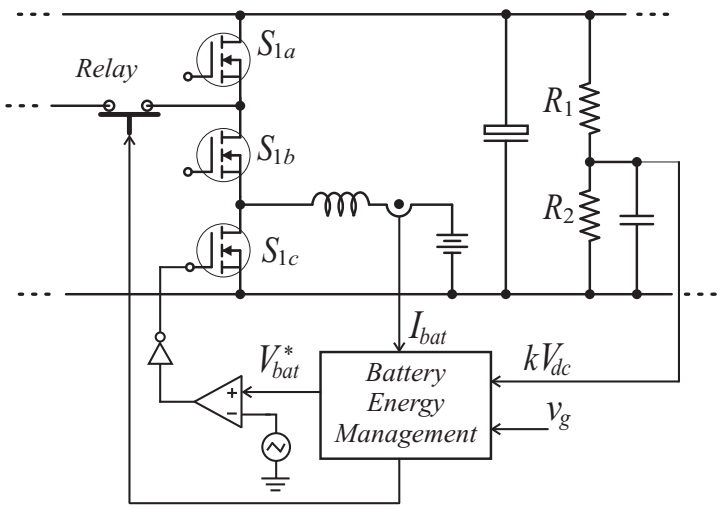

Fig. 2.4. Schematic for the battery energy management system.

turn, presents the control block diagram to control the dc-link capacitor voltage (V_{dc}) during the abnormal grid operation. In this case, a cascade control is employed to send the energy from the battery to the load. Notice that the output of the controller C_v will define reference of the battery current (I^*_{bat}) to keep the voltage V_{dc} under control. Such a reference current is compared to the measured current I_{bat}, and the output of the current controller defines V^*_{bat} for the PWM.

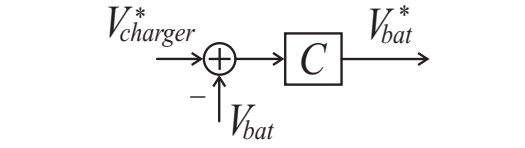

(a)

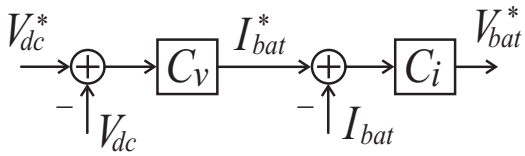

(b)

Fig. 2.5. (a) Battery voltage control. (b) Dc-link capacitor voltage control.

2.4 Simulated Results

The proposed UPS has been tested through simulation results. The parameters of the simulation is given by: 1) ac capacitors employed as voltage divider at the grid voltage of $3.3\mu F$, 2) inductors $L1$ and $L2$ of $60\mu H$, 3) dc-link capacitor of $1100\mu F$, 4) LCL output filter constituted by the two inductors and a capacitor of $60\mu H$ and $45F$, and 5) resistive load of 280. As shown in Fig. 2.6(a), by allowing the voltage v_{N0} to have a constant duty cycle of 0.5, the input grid voltage and current will be in phase (controlled power factor). The dc-link voltage across the capacitor is also constant, as shown in Fig. 2.6(b). Fig. 2.6(c) shows the load voltage and current as expected.

Fig. 2.7 shows the details about the power factor operation of the proposed converter. Fig. 2.7(a) presents the grid variables (v_g and i_g) as well as the inductor currents (i_{L1} and i_{L2}) for the positive half-cycle of the grid voltage. Fig. 2.7(b) shows the same variables as before for the negative half-cycle of the grid voltage.

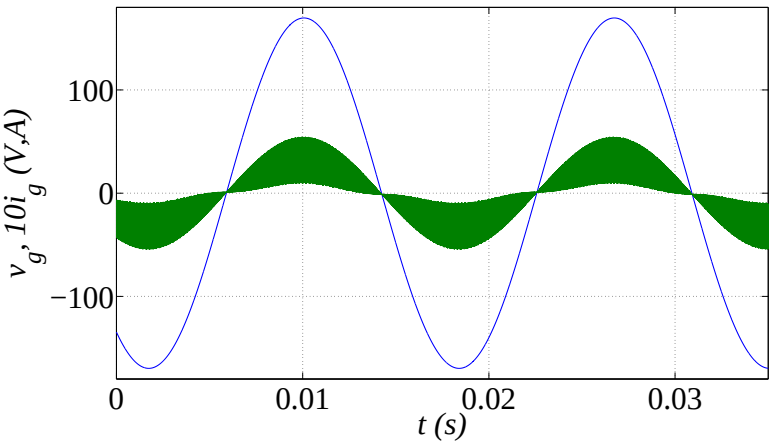

(a)

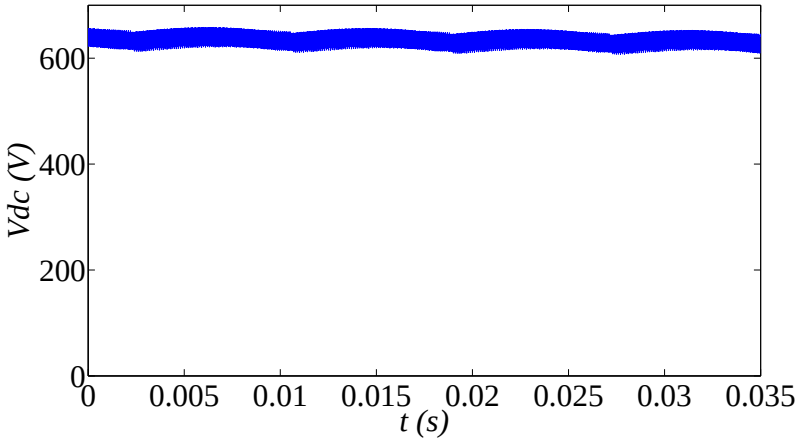

(b)

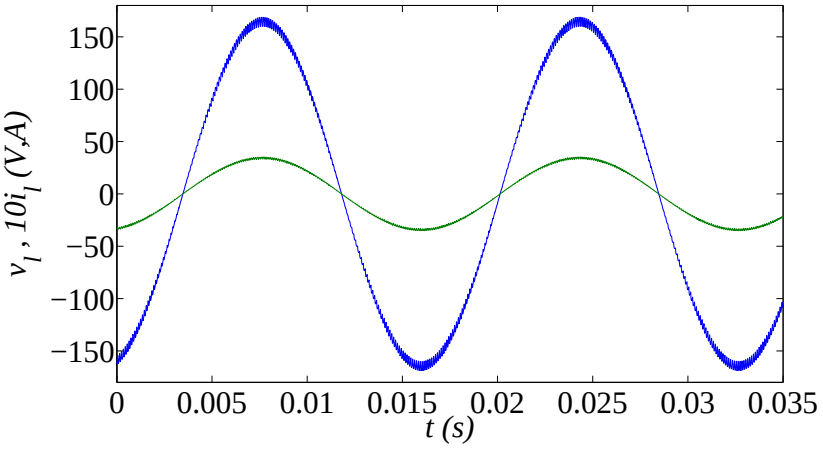

(c)

Fig. 2.6. Simulation results: (a) input power factor correction, (b) dc-link voltage, and (c) load voltage and current.

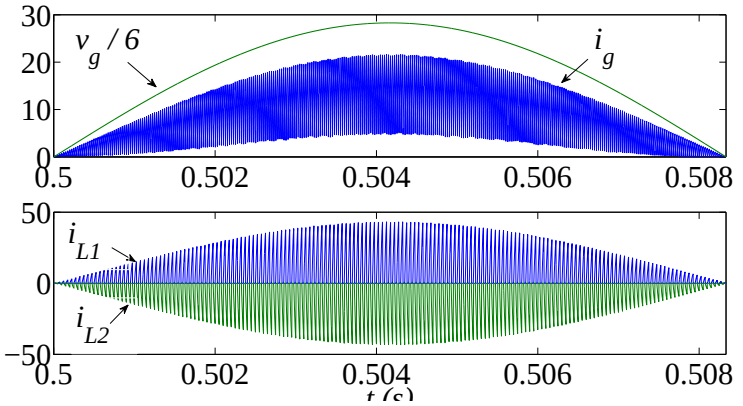

(a)

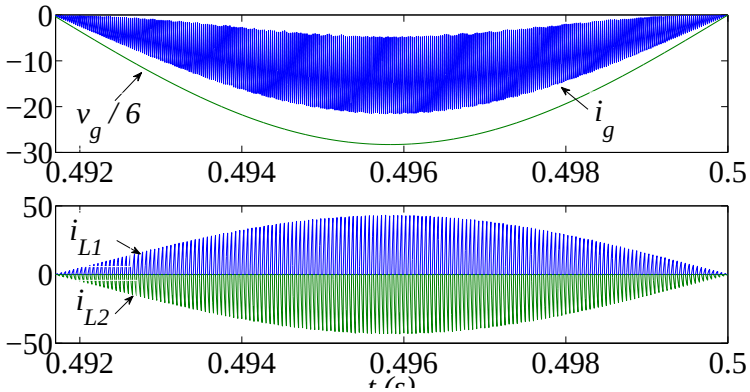

(b)

Fig. 2.7. Simulation results: (a) positive half-cycle of the grid voltage/current, and (b) negative half-cycle of the gird voltage/current.

3. OPTIMIZED SINGLE-PHASE BACK-TO-BACK CONVERTER FOR UPS APPLICATIONS

This section proposes a single-phase back-to-back converter [see Fig. 3.1] for applications in UPS systems with optimized operation in terms of either power losses reduction or better performance in terms of the quality of the waveform generated by the converter (lower total harmonic distortion of the grid current). The complete analysis presented in this thesis includes the converter model, its operation, the PWM strategy, dc-link capacitor voltage and grid current controls. Also, a comprehensive comparison between the proposed and conventional converter presented in Fig. 3.1 will be studied more in depth. Simulation results are presented to validate the theoretical study.

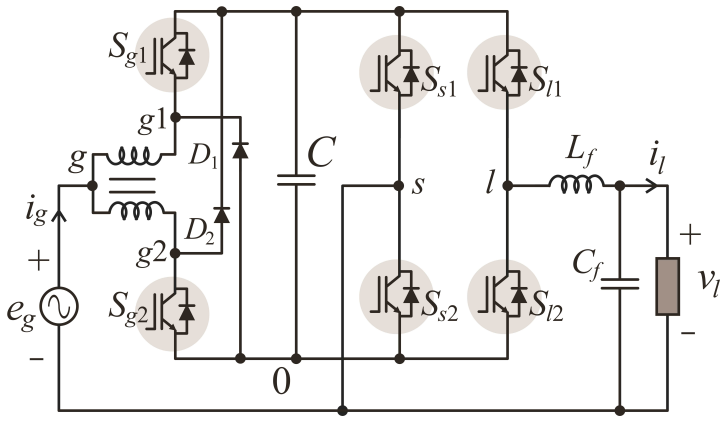

Fig. 3.1. The proposed back to back converter.

3.1 Principle of Operation and Model

The input side (rectifier) is made up of four switching power devices ($S_{g1} - S_{g2}$ and $S_{s1} - S_{s2}$), two diodes (D_1 and D_2) and one split-wound coupled inductor [35].

The legs constituted by the switches ($S_{s1} - S_{s2}$) will be shared with the inverter. The state of the all the switches can be represented by a binary variable, where $S_j = 0$ indicates an open switch and $S_j = 1$ indicates a closed switch (with $j = g_1$, g_2, s_1, s_2, l_1, and l_2). It is assumed that the currents in the coupled-windings are in continuous conduction mode, as highlighted in Fig. 2(a). Figs. 3.2(b), 3.2(c), 3.2(d), and 3.2(e) show equivalent circuits when the switches of the first leg ($S_{g1} - S_{g2}$) are equal to (0-0), (1-1), (0-1), and (1-0) respectively. The voltages v_{g10} and v_{g20} (voltages from the points g_1 and g_2 to zero) can be expressed as a function of the state of the switches, as shown below:

$$v_{g10} = S_{g1} v_c \tag{3.1}$$

$$v_{g20} = (1 - S_{g2}) v_c \tag{3.2}$$

This means that the converter can be modeled as shown in Fig. 2.1. In this figure, v_{s0} is the voltage from point s to zero and it is given by:

$$v_{s0} = S_{s1} v_c \tag{3.3}$$

where $S_{s1} = 1 - S_{s2}$, meaning that the switches S_{s1} and S_{s2} are complementary of each other, to avoid a short-circuit of the dc-link voltage across the capacitor (v_c). Then, the voltage v_{g0} is given by:

$$v_{g0} = \frac{1}{2}(v_{g10} + v_{g20}) \tag{3.4}$$

Once the voltages v_{g0} and v_{s0} were obtained, the AC voltage of the rectifier will be given by:

$$v_g = v_{g0} - v_{s0} \tag{3.5}$$

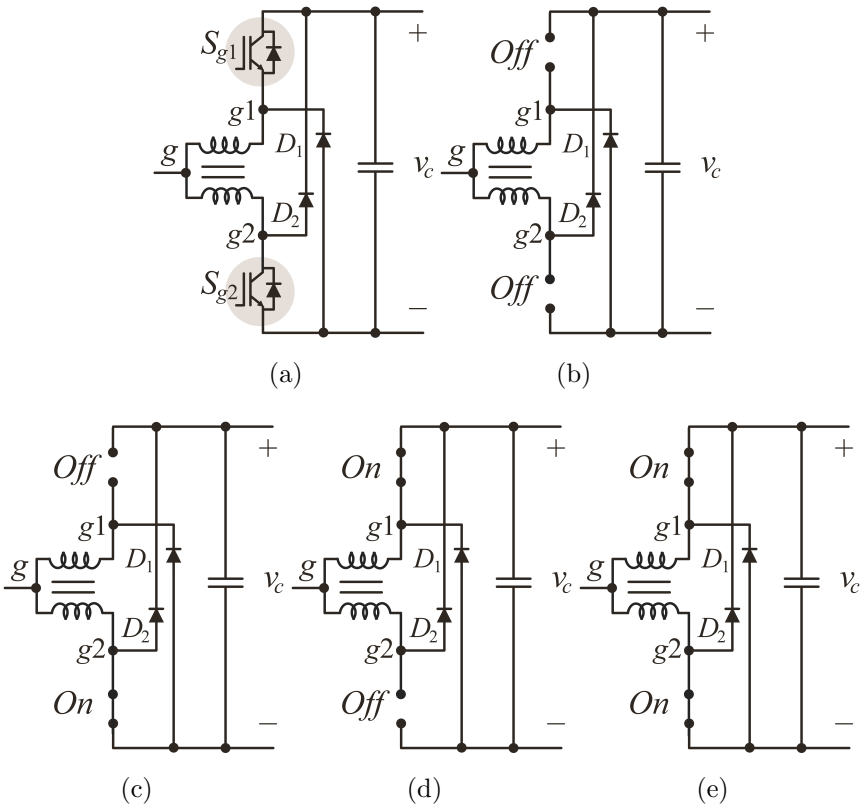

Fig. 3.2. (a) Operation in continuous conduction mode. (b) $S_{g1} = S_{g2} = 0$. (c) $S_{g1} = 0$ and $S_{g2} = 1$. (d) $S_{g1} = 1$ and $S_{g2} = 0$. (e)$S_{g1} = S_{g2} = 1$.

From equation (3.5), it is possible to model the converter as depicted in Fig. 3.3. Another important variable in this circuit is the inductor voltage (v_{ind}), which is used to guarantee continuous conduction mode, this voltage is given by:

$$v_{ind} = v_{g10} - v_{g20} \tag{3.6}$$

The inverter is modeled with the shared leg of S_{s1} and S_{s2}, and by the leg with the switches S_{l1} and S_{l2}, which allows:

$$v_{l0} = S_{l1} v_c \tag{3.7}$$

Then, load voltage (v_l) can be written as:

$$v_l = v_{l0} - v_{s0} \tag{3.8}$$

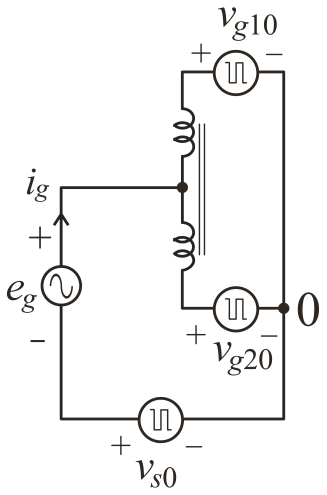

Fig. 3.3. Converter rectifier model.

3.2 PWM Strategy and Control Approach

As described in the rectifier model, both voltages v_g and v_{ind} were obtained from the pole voltages v_{g10}, v_{g20} and v_{s0}. In terms of control actions, there is a need to regulate two main variables, the dc link voltage v_c (at the output converter) and the grid current i_g must be sinusoidal with a power factor close to one at the input converter side. The cascaded closed loop control in Fig. 3.4 is used for this task, where the output of the C_V block (PI controller) will define the amplitude of the reference grid current I_g^*. The instantaneous reference grid current, i_g^*, is obtained from I_g^* multiplied by the output of a phased lock loop (PLL) block. The PLL's job is to provide a sinusoidal signal with an amplitude of 1, and that is in-phase with the grid voltage. The output of the current controller C_i defines the reference grid voltage v_g^* employed in the PWM strategy.

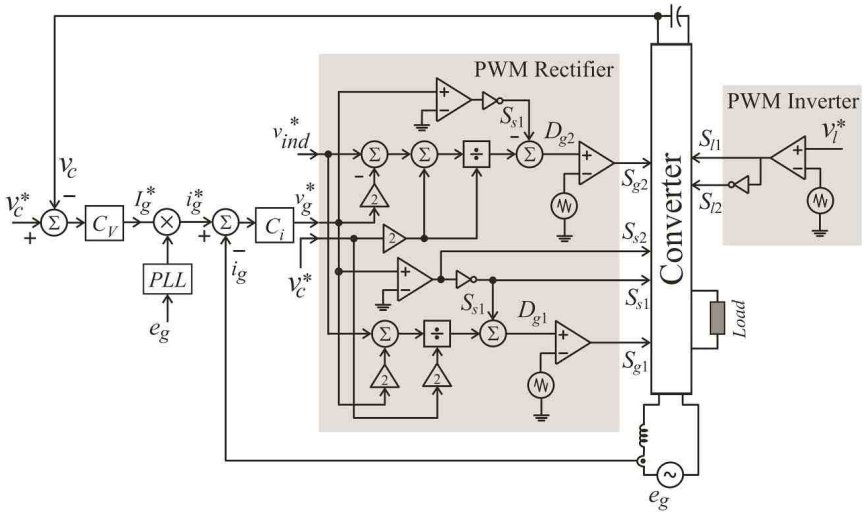

Fig. 3.4. PWM strategy employed for the control of the DC link voltage.

The gating signals S_{g1},S_{g2},S_{s1},and S_{s1} must be defined to generate the desired voltages v_g^* and v_{ind}^*. Since:

$$v_g^* = S_{g1}\frac{v_c}{2} + (1 - S_{g2})\frac{v_c}{2} - S_{s1}v_c \tag{3.9}$$

$$v_{ind}^* = S_{g1}v_c - (1 - S_{g2})v_c \tag{3.10}$$

Equations (3.9)-(3.10) are instantaneous expressions, which could be obtained throughout the average values in the switching period T_s. The duty cycle of each switch can be defined as the instantaneous switching states, as follows:

$$D_{g1} = \frac{1}{T_s}\int_t^{t+T_s} S_{g1}(t)dt \tag{3.11}$$

$$D_{g1} = \frac{1}{T_s}\int_t^{t+T_s} S_{g2}(t)dt \tag{3.12}$$

$$D_{s1} = \frac{1}{T_s}\int_t^{t+T_s} S_{s1}(t)dt \tag{3.13}$$

$$D_{s2} = \frac{1}{T_s}\int_t^{t+T_s} S_{s2}(t)dt = 1 - D_{s1} \tag{3.14}$$

This means that considering average values, equations (3.9) and (3.10) can be written as:

$$\frac{2v_g^*}{v_c} = D_{g1} + 1 - D_{g2} - 2D_{s1} \tag{3.15}$$

$$\frac{v_{ind}^*}{v_c} = D_{g1} + D_{g2} - 1 \tag{3.16}$$

And one possible solution from equations (3.15)-(3.16) for D_{g1} and D_{g2} would be:

$$D_{g1} = \frac{v_{ind}^* + 2v_g^*}{2v_c} + S_{s1} \tag{3.17}$$

$$D_{g2} = \frac{v_{ind}^* - 2v_g^*}{2v_c} + 1 - S_{s2} \tag{3.18}$$

Once the reference voltages v_g^*, v_{ind}^*,and v_c are known, the completion of the modulation scheme for S_{1s} must be defined following these rules: $S_{s1} = 1$ if $v_g^* < 0$ and $S_{s1} = 0$ if $v_g \leq 0$.

For the output converter side, the reference pole voltages defining the load voltage will have different frequencies. Then, v_{l0}^* must have a high switching frequency so that difference between v_{l0}^* and v_{s0}^* will have three levels. Fig. 3.4 well then be the complete analog solution for the PWM strategy presented in equations (3.17)-(3.18), together with the closed loop cascaded control strategy for the proposed rectifier.

3.3 Simulated Results and Experimental Results

The converter has been simulated using PSIM software. The load is given by $R = 39.6$, L_f=$50mH$, and C_f=$50\mu F$. The DC link voltage source is $375V$, and the switching frequency is $10KHz$. Fig. 3.5 (a) shows the simulation results for the rectifier variables, with the expected five levels for the voltage v_{gs} and sinusoidal grid current. Preliminary experimental results are presented in Fig. 3.5 (b).

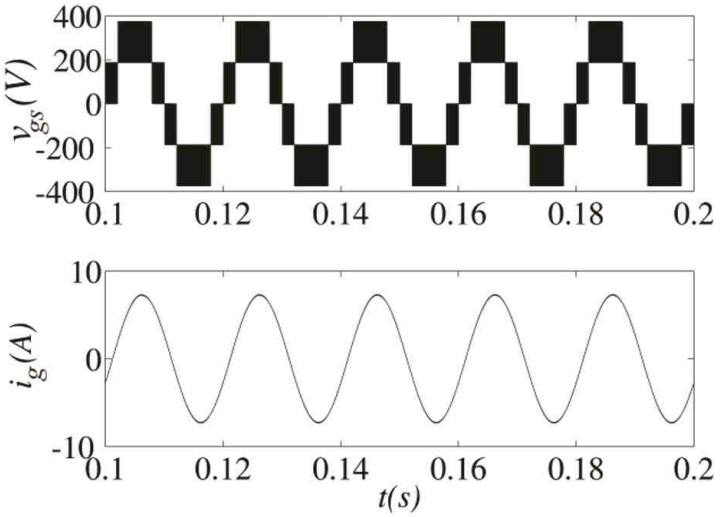

(a)

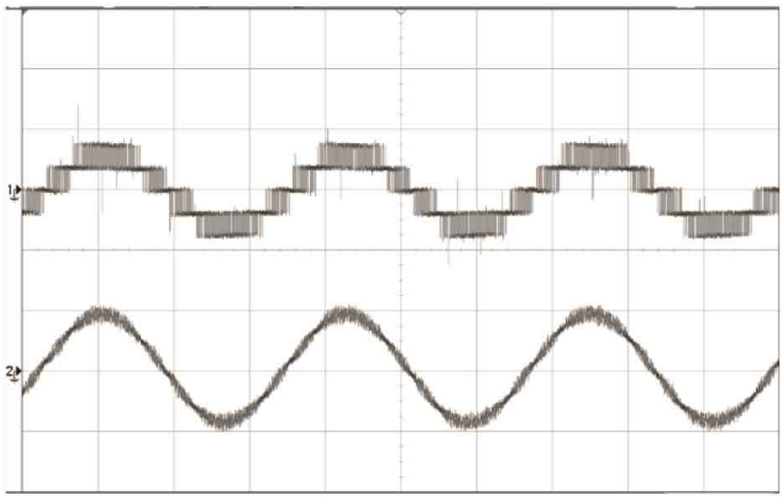

(b)

Fig. 3.5. (a) Simulation results, and (b) experimental results.

4. DELTA MICROINVERTERS

The purpose of the Delta Microinverter is to provide innovative solutions for installers and home owners of photovoltaic solar systems. Such a microinverter device is connected to directly to the solar panel and the utility grid. This device is able convert DC power from the solar panel, to AC power that is compatible with that delivered by the utility company. The Delta Microinverter will also guarantee that each solar module is operating at its maximum power point, and constantly provide information about the power that is delivered by each solar panel. The figure below (Fig. 4.1) shows the circuitry for the delta microinverter without the controller.

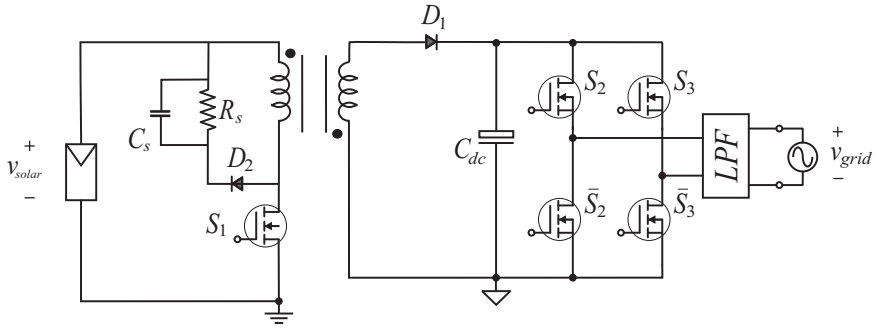

Fig. 4.1. Schematic of the Delta Microinverter.

4.1 DC-DC Converter

4.1.1 Flyback Topology

For typical microinverters, a boost converter is required to step up the voltage from the solar panels (typically from 18-35Vdc to 170Vdc in the United States). A flyback topology was used to implement the DC-DC boost converter for the Delta

Microinverter. A typical schematic for a flyback converter is presented in Fig. 4.2. The use of the transformer is to obtain a boosted voltage, depending on the ratio of the windings, and to achieve isolation from the input/output voltage.

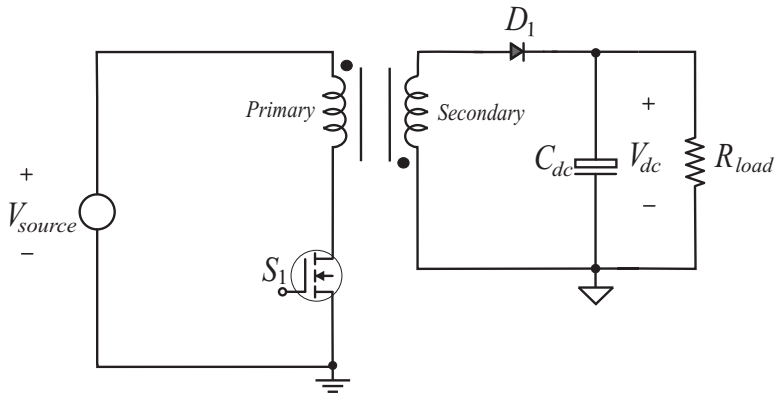

Fig. 4.2. Schematic of typical fly back converter.

Fig. 4.3 (a) and (b) show the two different modes of operation of the converter. In mode 1, the switch S_1 is off and the voltage of the primary of the transformer is connected to the input source. While the current and the magnetic flux increase in the primary, the secondary voltage induced of the transformer will be negative, keeping the diode D_2 off. Meanwhile, the capacitance would be discharging energy to the load. When the switch S_1 is on, the current of the input voltage will be zero, so the energy stored in the primary will be released through the secondary windings. This will cause the voltage at the secondary to be positive, which will forward-bias the diode so the energy goes through it to the load while also charging the capacitor.

4.1.2 Model and PWM Strategy

The switch S_1 plays an important role in achieving the desired voltage across the the capacitor C_{dc}. By controlling the duty cycle of this switch, the control of the voltage V_{dc} is guaranteed. A simple PI controller can be implemented for the control

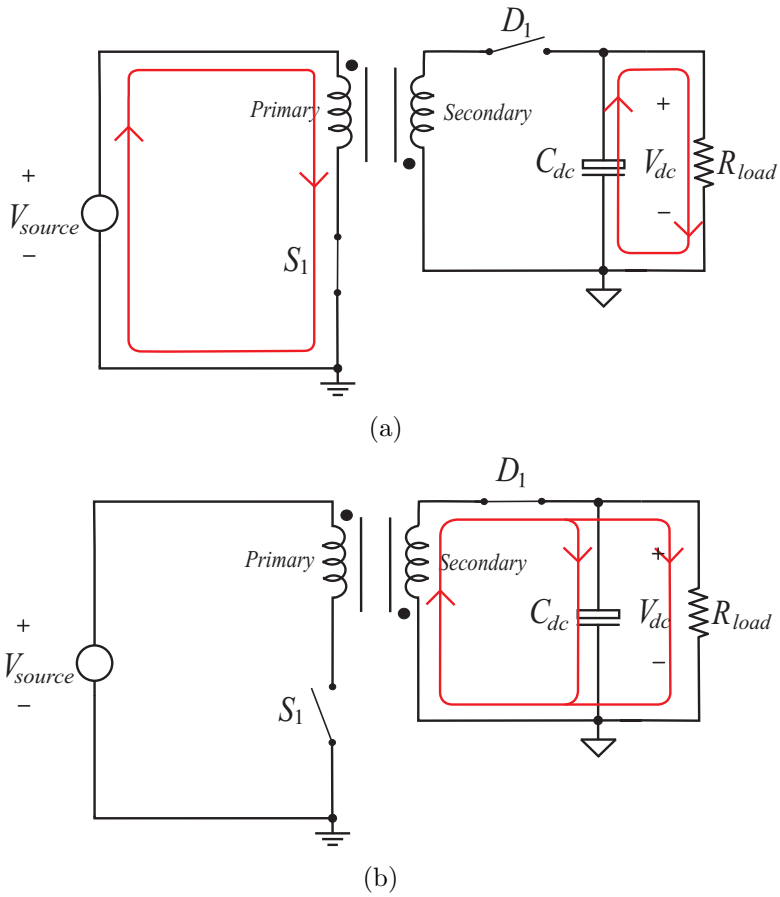

Fig. 4.3. (a) Mode 1, and (b) mode 2.

of this voltage, this is shown in Fig. 4.4. This is important part of the inverter, since the voltage at the input is continuously changing, the voltage across the capacitor C_{dc} must stay constant.

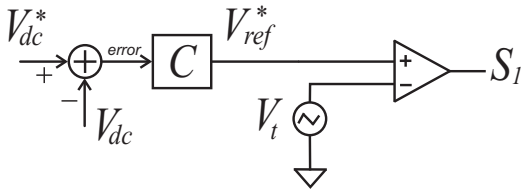

Fig. 4.4. PWM strategy for control of V_{dc}.

The voltage V_{dc}^* shown in Fig. 4.4 is the desired DC link voltage, where as V_{dc} is the actual voltage that needs to be controlled. The difference between the two voltages, error, is then the input of the PI controller labeled as C. The output of the PI controller will define the reference voltage V_{ref}^*, this will be compared with a triangular high frequency signal that decides the duty cycle of the switch S_1. Fig. 4.5 shows this comparison between the high frequency triangular signal and the reference voltage V_{ref}^*.

4.1.3 Snubber circuit

Snubber designs are quite important in plenty of applications. Not only do electrical systems needs a snubber for the voltage transients, but also for mechanical and fluid systems (extra forces and pressure transients) [62]. In the Delta application, a simple rectifier diode is in series with a parallel combination RC to form the snubber. This snubber is in parallel with the primary windings of the transformer, since they are usually associated with inductors. This is due to the fact that current of an inductor cannot change instantaneously, instead they are a continuous function of time. If the power switch was operating at a much higher frequency than $100MHz$,

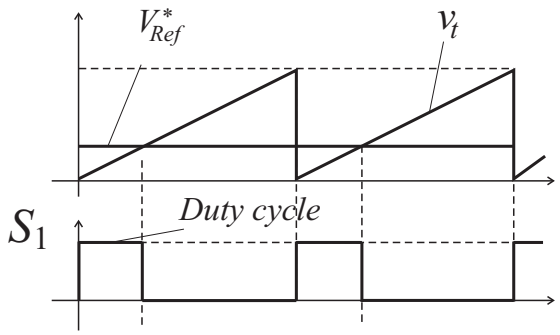

Fig. 4.5. Variable reference voltage V_{ref}^* defining the gating signal.

then the use of ultrafast or Schottky diodes may be used [44]. Fig. 4.6 shows the snubber circuit used in the Delta Microinverter.

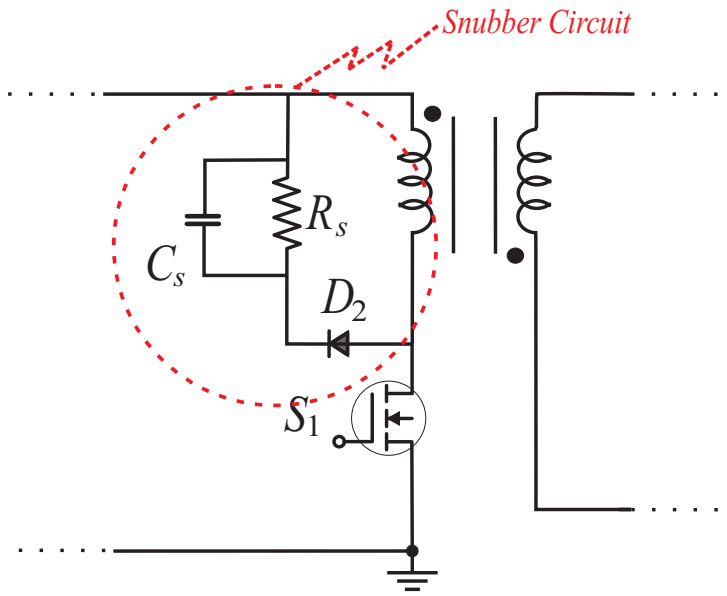

Fig. 4.6. The Diode/RC snubber circuitry for the Delta Microinverter.

4.2 DC-AC Inverter

4.2.1 H-Bridge Topology

Many methods of inverting DC voltage to AC exist, and the H-bridge topology is one of the most common ones used. The Delta also uses the H-bridge topology for inverting the controlled dc-link voltage V_{dc} to an ac voltage that is in phase with the grid. Fig. 4.7 shows the H-bridge topology which is implemented in the circuitry.

Some of the basics of this topology is that S_2 and $\overline{S}_2$ must be compliments of each other, so do S_3 and $\overline{S}_3$. This means that they cannot be on at the same time, avoiding short-circuit of the dc-link voltage. Table 4.1 shows the line-to-line voltage $V_{23} = V_2 - V_3$ with the corresponding switching state.

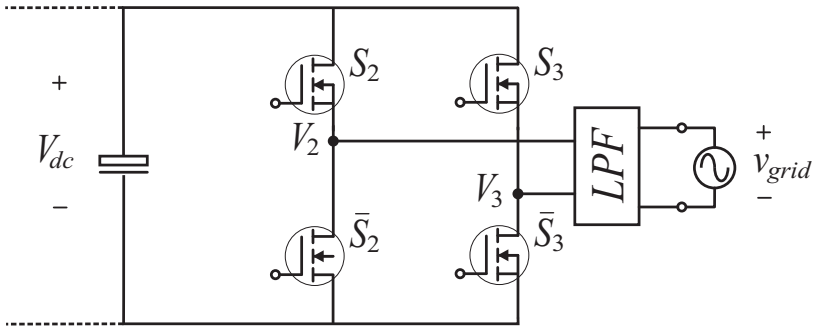

Fig. 4.7. H-bridge topology used in the Delta Microinverter.

Table 4.1.
The switching states of the H-bridge

States	S_2	S_3	V_{23}
1	0	0	0
2	0	1	$-V_{dc}$
3	1	0	V_{dc}
4	1	1	0

4.2.2 Model and PWM strategy

Guaranteeing the control of the output current is the most important part of the scheme. Since the voltage is defined by the grid, the current is what needs to be controlled in order to insure proper flow of power to the utility grid. Fig. 4.8 shows the complete control strategy used to guarantee control of the current.

First, the phase of the grid voltage v_g must be obtained in order to insure a

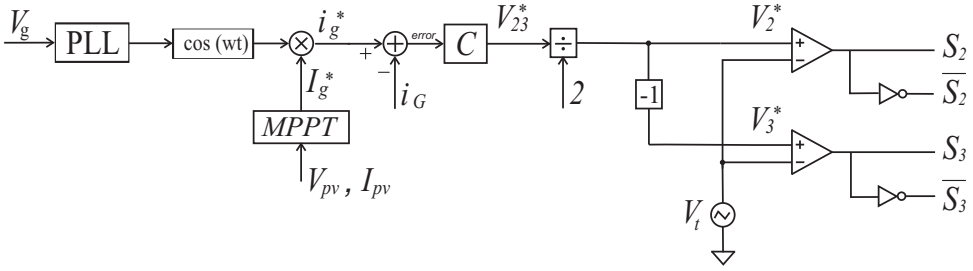

Fig. 4.8. PWM strategy for control of the grid currenti_g.

proper reference current i_g^*. This angle δ is obtained through a typical PLL scheme, which will be used to define a sinusoidal signal that is in-phase with the grid voltage. The amplitude of the reference grid current I_g^* will be multiplied by the sinusoidal signal to obtain the reference grid current i_g^*. To insure the control of the grid current i_g, the difference of i_g^* and i_g will define an error for the PI controller labeled C. The controller well set the reference line-to-line voltages V_{23}^* that will be used to define the pole voltages. This can be seen from equation 4.1 below:

$$V_{23}^* = V_2^* - V_3^* \tag{4.1}$$

Then, one solution would be to make:

$$V_2^* = \frac{V_{23}^*}{2} \tag{4.2}$$

and,

$$V_3^* = -\frac{V_{23}^*}{2} \tag{4.3}$$

This way, the reference pole voltages will define the state of the switches, as shown in Fig. 4.8.

If the line-to-line voltage is to be represented as a pulsating voltage, and the LPF as just a simple inductance, then the right side of 4.7 can be represented as shown in

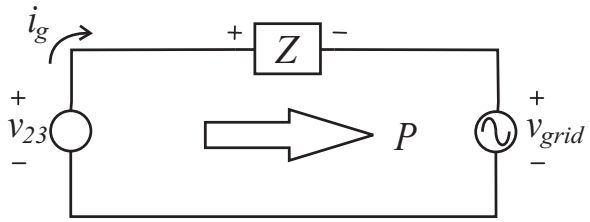

Fig. 4.9. Simple representation of the output side.

Fig. 4.9. In this figure, Z will be the impedance of the inductance defined as $R+jX$. The equation of the current can be seen as follows:

$$i_g = \frac{v_{23} - v_{grid}}{Z} \tag{4.4}$$

Where $v_{23} = V_{23}e^{j\delta}$ and $v_{grid} = V_{grid}e^{j\beta}$. If the grid voltage is set to be the reference voltage, then the angle β can be considered 0 and then equation 4.4 can be written as:

$$i_g = \frac{V_{23}\, e^{j\delta} - V_{grid}}{R + jX}$$

$$i_g = \frac{V_{23}\, cos(\delta) + j\, V_{23}\, sin(\delta) - V_{grid}}{R + jX} \tag{4.5}$$

As in most power systems, the small resistance R which is associated with the inductance or capacitance is neglected in calculation (shown in [63]) resulting in:

$$i_g = \frac{V_{23}\, cos(\delta) + j\, V_{23}\, sin(\delta) - V_{grid}}{jX}$$

$$i_g = \frac{V_{23}\, cos(\delta) + j\, V_{23}\, sin(\delta) - V_{grid}}{jX}\,\frac{j}{j}$$

$$i_g = \frac{V_{23}\, sin(\delta) - j[\, V_{23}\, cos(\delta) - V_{grid}]}{X}$$

$$i_g = \frac{V_{23}\, sin(\delta) - j[\, V_{23}\, cos(\delta) - V_{grid}]}{X}$$

$$i_g = \frac{V_{23}\, sin(\delta)}{X} - \frac{j[\, V_{23}\, cos(\delta) - V_{grid}]}{X} \tag{4.6}$$

And the real power that is delivered to the grid can be seen as:

$$P = Re[v_{grid}\, i_g^*] \tag{4.7}$$

where Re denotes the real part of a complex number and the * here denotes the complex conjugate. Then it is evident that the power P that is supplied by v_{23} is:

$$P = \frac{V_{grid}\, V_{23}}{X}\, sin(\delta) \tag{4.8}$$

The approach of presenting power flow in a triangle form has been presented in [45]. Considering the phasor diagram (Fig. 4.10) of the simplified circuit shown in Fig. 4.9. If the current i_g has the same angle of the grid voltage v_{grid}, the resulting angle δ of v_{23} will be positive. This means that equation 4.8 will always be positive, and the power will be absorbed by v_{grid}. Another method of determining the power flow direction with the phase angle between the current and the voltage was presented in [46].

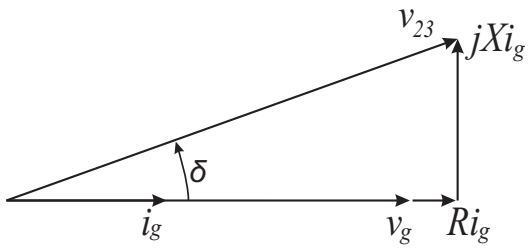

Fig. 4.10. Phasor diagram of the simplified circuit in fig 4.9.

4.2.3 LPF

A LCL low pass filter (LPF) is chosen for this design, and it is to achieve a better current waveform than a L type filter as in typical voltage source inverters [49], [50]. LC type filters are affected by the change in the resonance frequency throughout time, therefore they are disregarded [52]. Other research shows the effects of the grid inductance on the LC filter, and why this type of filter should be avoided. One of the most important requirements for microinverters (grid-tie) is that the quality of the current injected to the utility grid must have minimum distortion. Details about proper and systematic design of a LCL LPF is discussed in [47]. Fig. 4.11

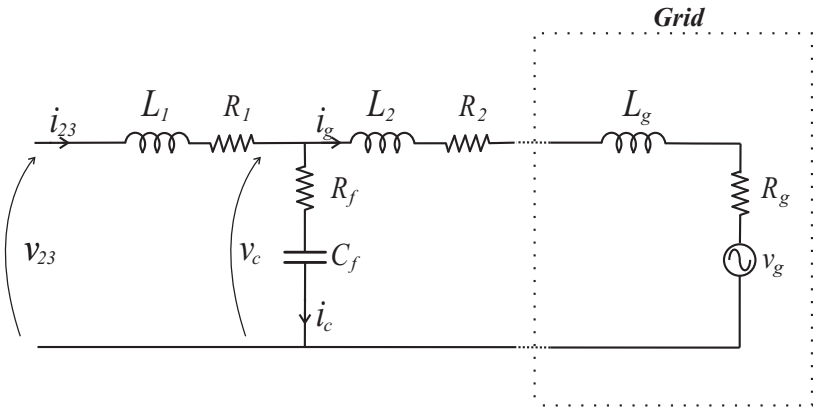

Fig. 4.11. Model of the LPF.

shows a per phase equivalent circuit as depicted in [48]. Since the grid voltage v_g should be an ideal voltage source (it is a short-circuit for harmonic frequencies), it will be considered 0 for the calculation of the transfer function of the LPF. One KCL equation can then be derived in the s domain, such as:

$$i_{23} = i_g + i_c \tag{4.9}$$

And the currents can be defined as:

$$i_{23} = \frac{v_{23} - v_c}{R_1 + sL_1} \tag{4.10}$$

$$i_c = \frac{v_c}{R_c + \frac{1}{sC_f}} \tag{4.11}$$

and,

$$i_g = \frac{v_c}{(R_2 + R_g) + s(L_g + L_2)} \tag{4.12}$$

Since the goal is to achieve the transfer function $\frac{i_g}{v_{23}}$, equation 4.10 can be redefined so that all the currents are with respect to i_g.

$$v_{23} = i_{23}(R_1 + sL_1) + v_c \tag{4.13}$$

And setting v_c of equation 4.11 and 4.12 equal, the current i_c can be written with respect to i_g.

$$i_g[(R_2 + R_g) + s(L_g + L_2)] = i_c(R_c + \frac{1}{sC_f})$$

$$i_c = i_g \frac{(R_2 + R_g) + s(L_g + L_2)}{(R_c + \frac{1}{sC_f})}$$

$$i_c = i_g \frac{s\,C_f(R_2 + R_g) + s^2\,C_f(L_g + L_2)}{(s\,C_f R_c + 1)} \tag{4.14}$$

Then, plugging in 4.14 into 4.9 and then to the redefined equation of 4.10 while solving for v_c from 4.12 yields to:

$$v_{23} = i_g \frac{[s\,C_f(R_2 + R_g) + s^2\,C_f(L_g + L_2)](R_1 + s\,L_1)}{s\,R_c C_f + 1} + i_g(R_1 + s\,L_1)$$

$$+ i_g[(R_2 + R_g) + s(L_g + L_2)] \tag{4.15}$$

After taking a common denominator of the right side,

$$v_{23} = \frac{i_g[s^3\,\alpha + s^2\,\beta + s\,\gamma + \delta]}{1 + s\,R_c C_f} \tag{4.16}$$

where,

$$\alpha = L_1 C_f(L_g + L_2)\,,$$

$$\beta = C_f[R_1(L_g + L_2) + L_1(R_2 + R_g + R_c) + R_c(L_g + L_2)]\,,$$

$$\gamma = C_f[R_1(R_2 + R_g) + R_c(R_2 + R_g) + R_c R_1] + L_1 + L_2 + L_g\,,$$

and,

$$\delta = R_1 + R_2 + R_g\,.$$

Finally, rearranging equation 4.16 can then result to:

$$\frac{i_g}{v_{23}} = \frac{1 + s\,R_c C_f}{s^3\,\alpha + s^2\,\beta + s\,\gamma + \delta} \tag{4.17}$$

The transfer function was calculated in order to plot the bode diagrams, which are useful in analyzing the system's response to different values of L_1, C_f, and L_2.

4.3 Triangular Shape

4.3.1 Comparison with other Solutions

The market for the microinverters is growing every year. One significant notice for these devices was the shape of them, they are all square shaped with at least 2 screws attaching them to the solar panel or a mounting bracket. The goal for the Delta Microinverter was not only to have a very efficient circuit, but also to provide better solutions for the installers of the solar system. Thats where the idea of the patented triangular shape came from. It is evident from Fig. 4.13 (b) that a triangular shape with one screw would be of more convenience to the solar installers. Fig. 4.12 [57–61] shows other brands of microinverters, to give an idea of how much time can be saved with this new shape.

4.3.2 Schematic and Printed Circuit Board

For the Delta Microinverter, the Printed Circuit Board (PCB) was made with the software Altium. A schematic must be made (Fig. 4.3.2) to help with the convenience of checking different points once the PCB has been printed. It also helps in connecting all the nodes of the PCB layout, which becomes more complex as the system grows. In the schematic section, each component can be edited so that the foot print can match the actual size of the part. Once the PCB layout has finished, gerber and NC drill files must be made in order for companies to make the PCB. Fig. 4.15 shows the final PCB layout that was made for the prototype of the Delta Microinverter.

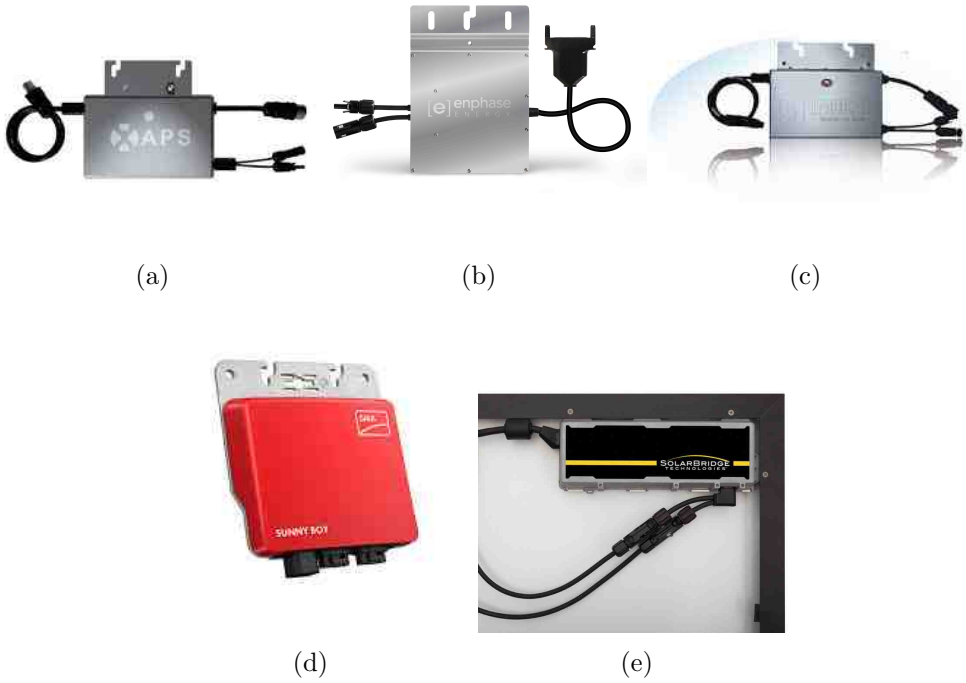

(a) (b) (c)

(d) (e)

Fig. 4.12. (a) APS, (b) Enphase, (c) Involar, (d) SMA, and (e) Solar Bridge.

4.3.3 Enclosure

The enclosure of the Delta Microinverter consists of two parts; the heat sink base, and the cover. The design of whole enclosure was made with Google's free 3D designing software SketchUp. This can be seen below in Fig. 4.16 (a)-(d). Two different companies were used to make the actual enclosure. The first one was for the heat sink, it was through a company called eMachineShop, and they specialize in making custom aluminum extrusions. eMachineShop offers plenty of in depth specification regarding the type of metal intended for use, and the quality of the finish. The cover was made through a 3D printing company called Sculpteo. Sculpteo offers a variety of different plastic finishes and colors. Both companies accept file extensions directly created from the Google SketchUp software. Fig. 4.17 shows more pictures of the first prototype of the Delta Microinverter.

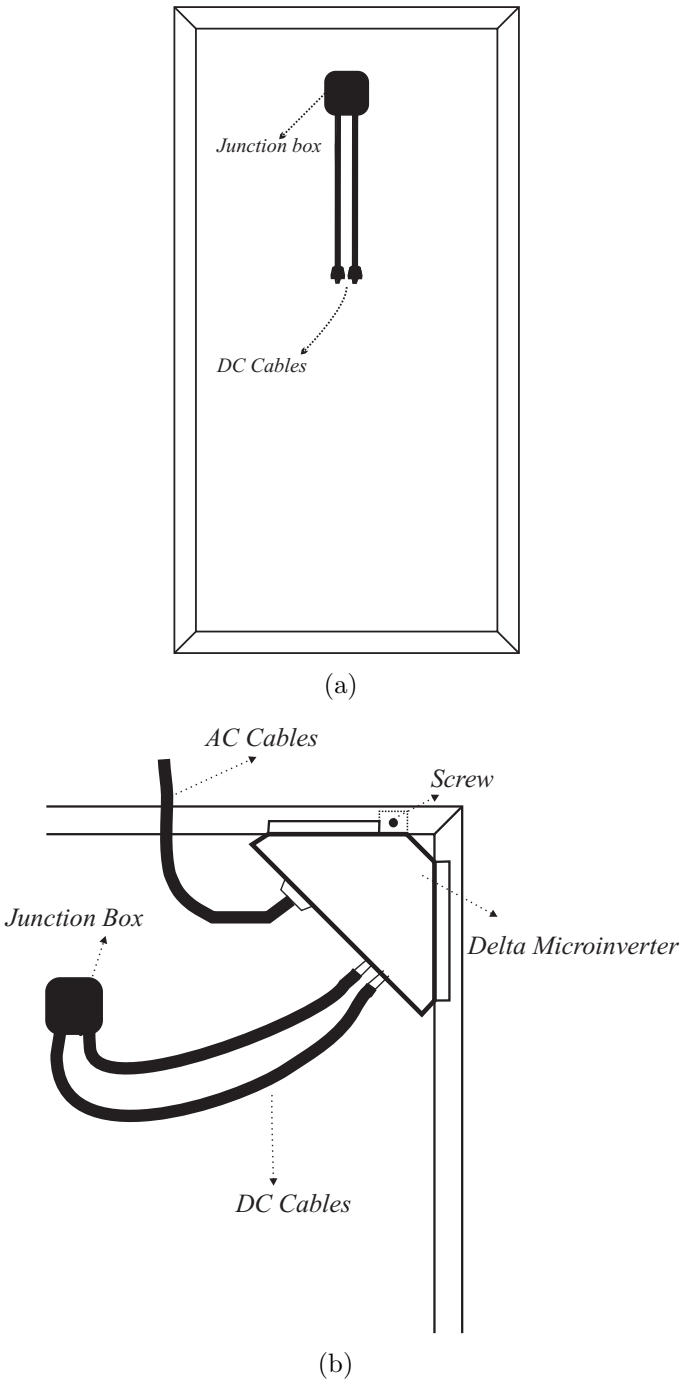

Fig. 4.13. (a) Back view of a solar panel. (b)Proposed Delta Microinverter setup.

4.4 Simulation and Experimental Results

The Delta Microinverter was simulated using the software PSIM for closed loop control scheme, while the experimental results were done in open loop (Fig. 4.18).

The same conditions were used for the test in PSIM as the real experimental results, such as: 400Ω resistive load, inductance of $100\mu H$ for each inductor (total of 3) used in the LPF, capacitance of $100\mu F$ for each capacitor used in the LPF, and input voltage of $20Vdc$. As shown in Fig. 4.19, the boost converter was able to step up the voltage to $190Vdc$ at the dc-link. Fig. 4.20 shows the current from the inputs side, while Fig. 4.21 (a) and (b) show the PWM frequency difference of the boost converter and the inverter. The outputs side after the LPF was a pure sine wave with $60Hz$ frequency and $120Vrms$ (Fig. 4.22). Another thing to note was the use of a film capacitor of $1F$ across the dc-link voltage during the experiment. This capacitor got rid of the high frequency ripple, as evident from Fig. 4.23 (a) and (b).

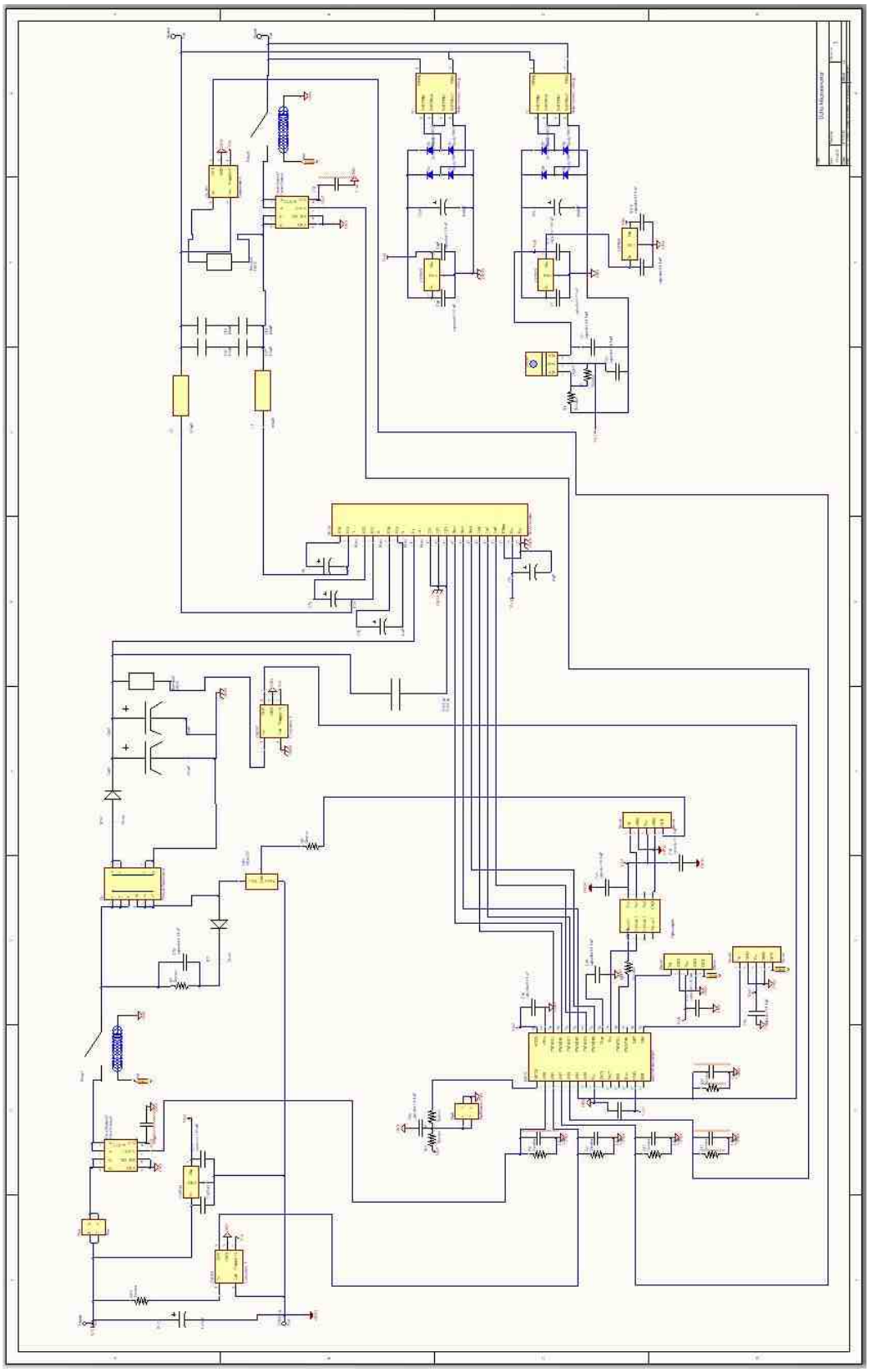

Fig. 4.14. Schematic of the Delta Microinverter.

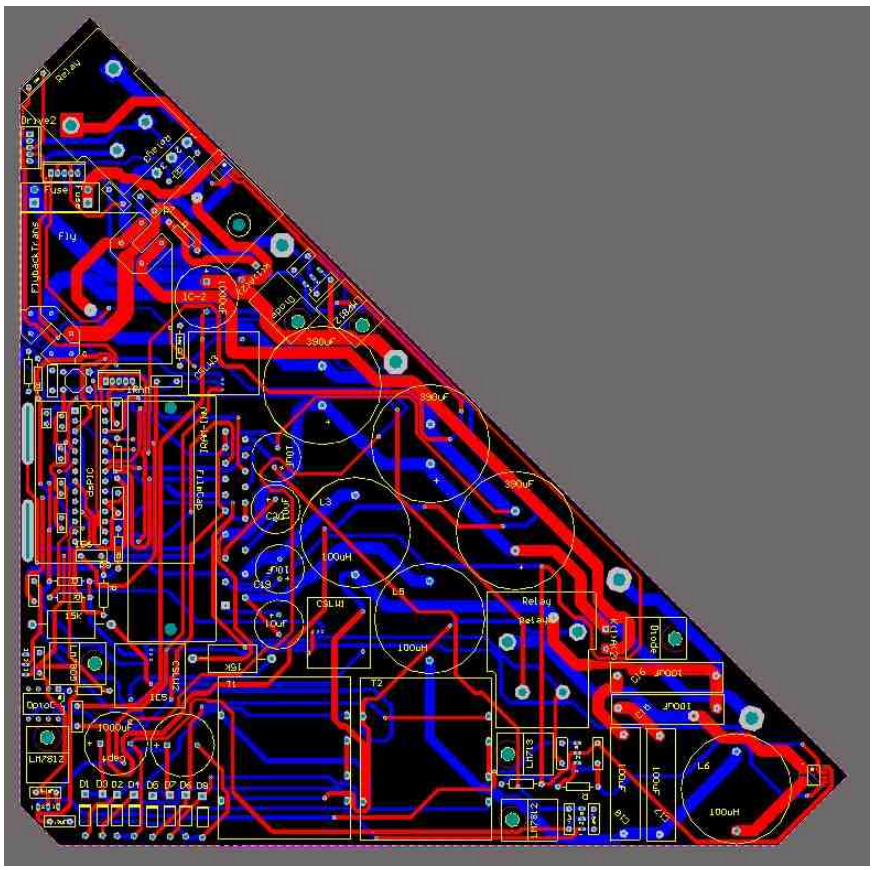

Fig. 4.15. PCB layout of the Delta Microinverter.

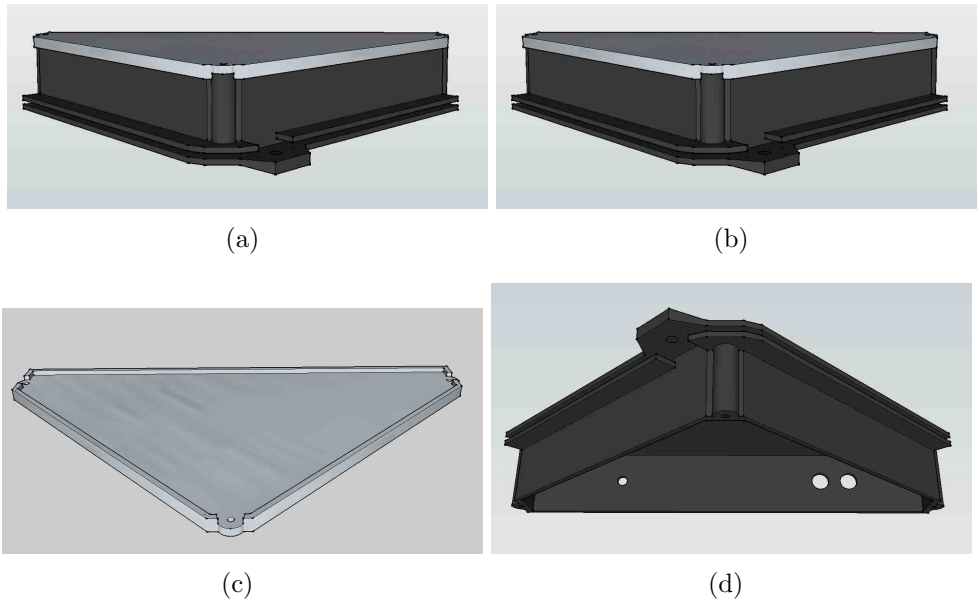

(a) (b)

(c) (d)

Fig. 4.16. 3D Design made in Google SketchUp: (a)-(b) Different top views, (c) plastic cover, and (d) aluminum heat sink.

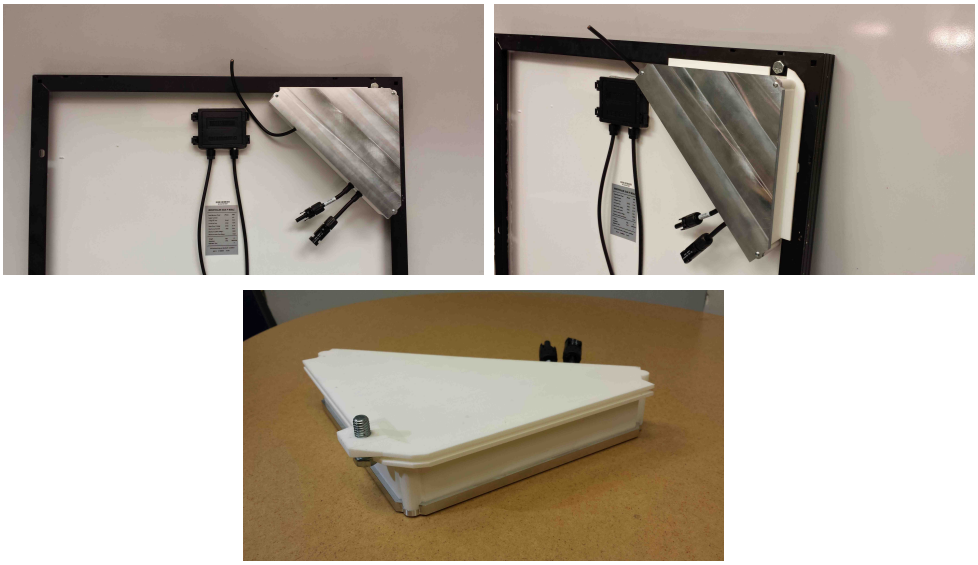

Fig. 4.17. Photos showing the prototype of the Delta Microinverter.

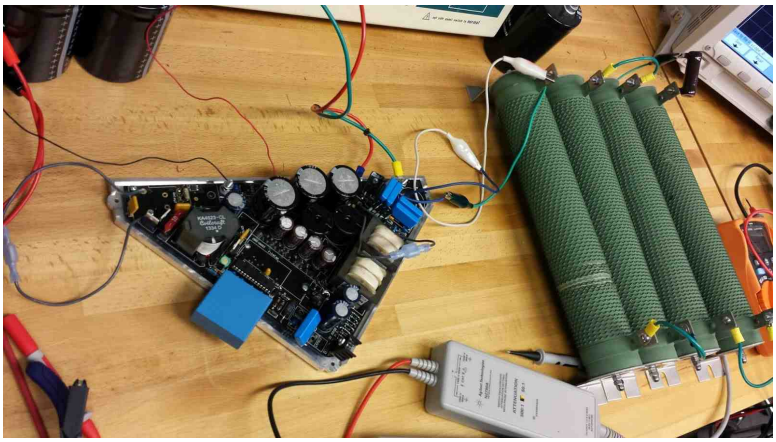

Fig. 4.18. The Delta prototype during testing.

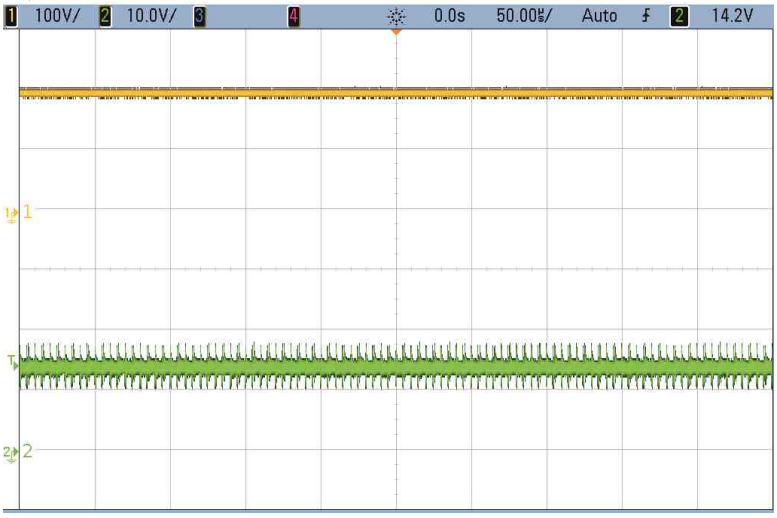

Fig. 4.19. Experimental results showing the boost converter: the first signal (yellow) is the boosted voltage, and the second (green) is the input.

Fig. 4.20. Current flowing from the solar panel.

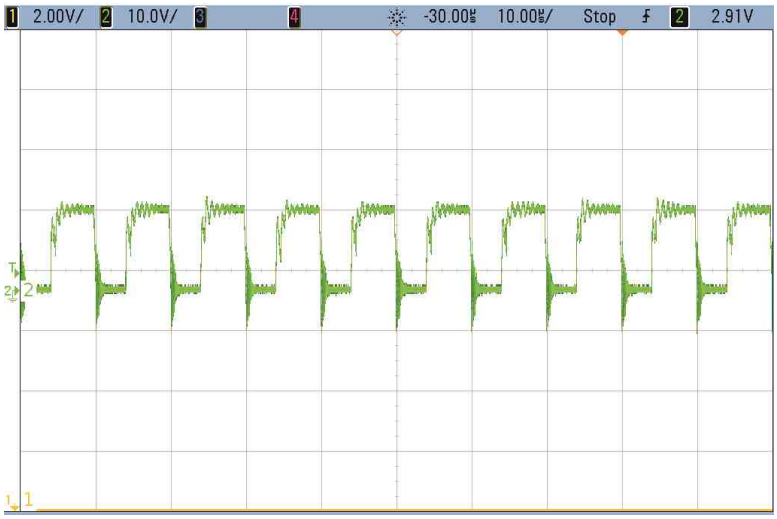

(a)

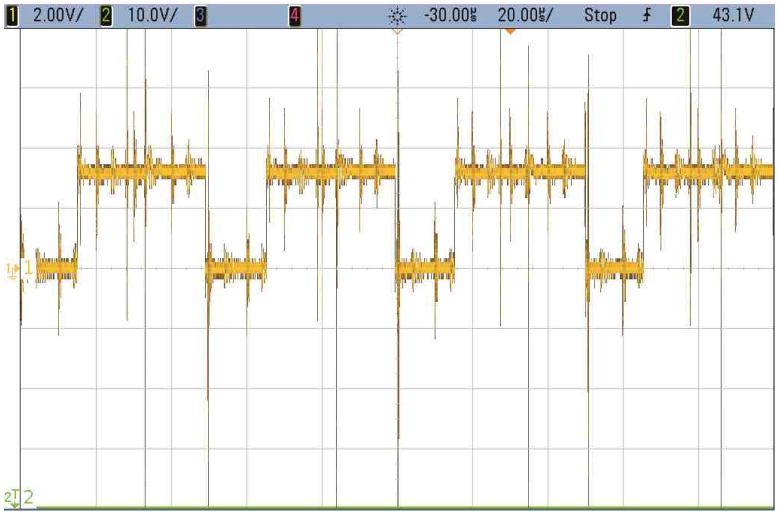

(b)

Fig. 4.21. (a) The signal applied to the MOSFET at the inputs side($100kHz$), and (b) signal applied to one of the switches on the inverters side ($20kHz$).

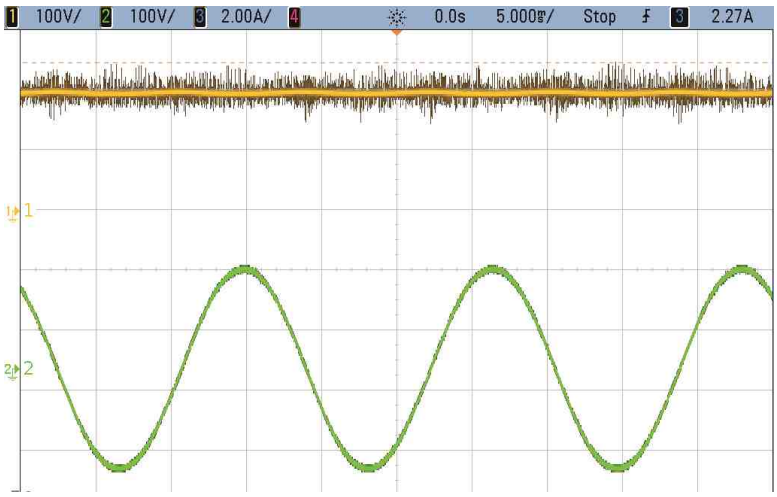

Fig. 4.22. The output of the LPF is shown in green, and the dc-link voltage is the yellow signal.

(a)

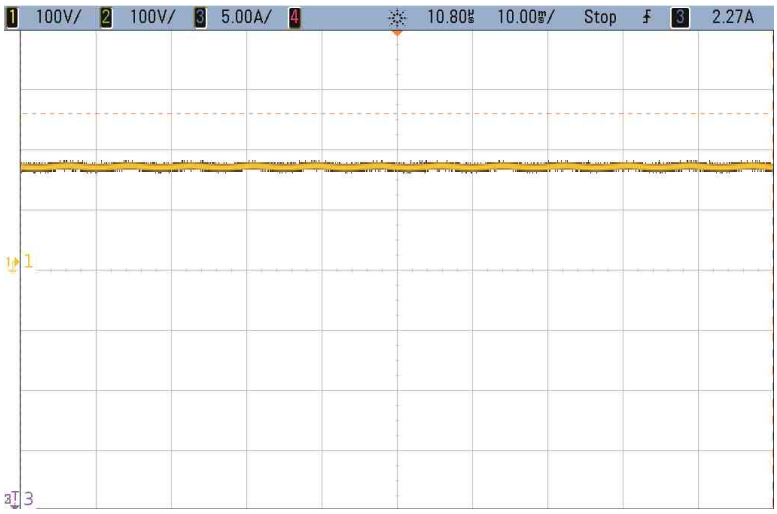

(b)

Fig. 4.23. (a) The dc-link Voltage without a film capacitor, and (b) shows the dc-Link with the film capacitor.

5. SUMMARY

The thesis proposed offers power electronic solutions for UPS and grid-tie inverters. One solution was for an on-line UPS system based on the integrated power electronics converter. The proposed converter allows the control of the input power factor, manages battery operation with backup operation in the case of utility power outage. The main advantages of the proposed UPS are active power factor correction (PFC) without any feedback control, and integrated functions of the battery charger circuit and PFC by using only three power switches. Details regarding the operation modes of the system and modulation strategy were presented. Simulation results are presented to validate the theoretical expectations.

The second proposed topology offers optimized waveforms generated by the converter and less power losses. Analysis of the converter model, its operation, PWM strategy, and control of the grid current and dc-link voltage was presented. Simulation results validate the theoretical studies, and preliminary experimental results were also presented.

Finally, the proposed grid-tie microinverter offers great technology and a new patented shape. It provides great efficiency and ease of installation compared to current competitors. A closed loop controlled scheme of the dc-ac converter is in experimental trails in accordance with theoretical studies. It will also guaranty that the input dc voltage is operating at its maximum power point. Experimental results of the open-loop tests where presented to validate the prototype in operation. The next generation of this prototype will include another patented circuitry for the dc-ac converter [53] that is able to achieve better efficiency.

REFERENCES

REFERENCES

[1] P. Angays, "What to do if you are afraid of the dark: recommendations for the design of electrical backup systems," *Industry Applications Magazine, IEEE*, vol. 19, no. 1, pp. 49-59, February 2013.

[2] F. Forest, T. A. Meynard, J. J. Huselstein, D. Flumian, C. Rizet, A. Lacarnoy, "Design and characterization of an eight-phase-137-kW intercell transformer dedicated to multicell dcdc stages in a modular UPS," *IEEE Transactions on Power Electronics*, vol. 29, no. 1, pp. 45-55, January 2014.

[3] U. K. Jethwa, R. K. Bansal, N. Date, R. Vaishnav, "Comprehensive load-shedding system," *IEEE Transactions on Industry Applications*, vol. 46, no. 2, pp. 740-749, March-April 2010.

[4] H. Pinheiro, P. Jain, G. Joos, "Design procedure for UPS based on series-parallel resonant converters," *Power Electronics Specialists Conference, 1999. PESC 99. 30th Annual IEEE*, vol. 2, pp. 1005-1010.

[5] O. M. Zhitkov, A. G. Garganev, A. G. Azarov, "Application of the uninterruptible power supply systems in medicine," *Modern Techniques and Technology, 2000. MTT 2000. Proceedings of the VI International Scientific and Practical Conference of Students, Post-graduates and Young Scientists*, pp. 216-217, 2000.

[6] S. Junlakarn, M. Ilic, "Distribution System Reliability Options and Utility Liability," *IEEE Transactions on Smart Grid*, vol. 5, no. 5, pp. 2227-2234, September 2014.

[7] S. Anand, S. K. Gundlapalli, B. G. Fernandes, "Transformer-less grid feeding current source inverter for solar photovoltaic system," *IEEE Transactions on Industrial Electronics*, vol. 61, no. 10, pp. 5334-5344, October 2014.

[8] Y. Wang, F. Wang, "Novel three-phase three-level-stacked neutral point clamped grid-tied solar inverter with a split phase controller," *Transaction on Power Electronics*, vol. 28, no. 6, pp. 2856-2866, June 2013.

[9] J. Sun, "Impedance-Based Stability Criterion for Grid-Connected Inverters," *IEEE Transactions on Power Electronics*, vol. 26, no. 11, pp. 3075-3078, November 2011.

[10] L. Aarniovuori, A. Kosonen, P. Sillanpaa, M. Niemela, "High-Power Solar Inverter Efficiency Measurements by Calorimetric and Electric Methods," *IEEE Transactions on Power Electronics*, vol. 28, no. 6, pp. 2798-2805, June 2013.

[11] H. Chiu, Y. Lo, C. Yang, S. Cheng, C. Huang, C. Chuang, M. Kuo, Y. Huang, Y. Jean, and Y. Huang, "A module-integrated isolated solar microinverter," *IEEE Transactions on Industrial Electronics*, vol. 60, no. 2, pp. 781-788, February 2013.

[12] J. Wu, and C. Chou, "A Solar Power Generation System With a Seven-Level Inverter," *IEEE Transactions on Power Electronics*, vol. 29, no. 7, pp. 3454-3462, July 2014.

[13] C. Yang, K. Smedley, "Three-phase boost-type grid-connected inverter," *IEEE Transactions on Power Electronics*, vol. 23, no. 5, pp. 2301-2309, September 2008.

[14] T. Ostrem, W. Sulkowski, L. E. Norum, and C. Wang, "Grid connected photovoltaic (PV) inverter with robust phase-locked loop (PLL)," *Transmission & distribution Conference and Exposition: Latin America, 2006. TDC '06. IEEE/PES*, pp. 1-7, August 2006.

[15] L. Liu, Y. Zhou, and H. Li, "Coordinated active and reactive power management implementation based on dual-stage PLL method for grid-connected PV system with battery," *Energy Conversion Congress and Exposition (ECCE), 2010 IEEE*, pp. 328-335, September 2010.

[16] M. Ciobotaru, R. Teodorescu, and F. Blaabjerg, "Control of single-stage single-phase PV inverter," *European Conference on Power Electronics and Applications*, pp. 10. 2005.

[17] P. Chaweewat, J. G. Singh, W. Ongsakul, and A. K. Srivastava, "Synchronization control and droop control of microgrid operation," *2014 International Conference and Utility Exhibition on Green Energy for Sustainable Development (ICUE)*, pp. 1-7, March 2014.

[18] O. A. Soysal, and H. S. Soysal, "Case study: performance of a small grid-tie wind-solar generation system," *PES General Meeting — Conference & Exposition, 2014 IEEE*, pp. 1-5, July 2014.

[19] H. M. Abdar, A. Chakraverty, D. H. Moore, J. M Murray, and K. A. Loparo, "Design and implementation a specific grid-tie inverter for an agent-based microgrid," *Energytech, 2012 IEEE*, pp. 1-6, May 2012.

[20] S. Ozturk, and I. Cadirci, "DSPIC microcontroller based implementation of a flyback PV microinverter using direct digital synthesis," *Energy Conversion Congress and Exposition (ECCE), 2013 IEEE*, pp. 3426-3433, September 2013.

[21] H. Haibing, S. Harb, N. H. Kutkut, Z. J. Shen, and I. Batarseh, "A single-stage microinverter without using eletrolytic capacitors," *IEEE Transactions on Power Electronics*, vol. 28, no. 6, pp. 2677-2687, June 2013.

[22] S. Harb, M. Kedia, Z. Haiyu, and R. S. Balog, "Microinverter and string inverter grid-connected photovoltaic system A comprehensive study," *2013 IEEE 39th Photovoltaic Specialists Conference (PVSC)*, pp. 2885-2890, June 2013.

[23] J. R. Dreher, F. Marangoni, L. Schuch, M. L. da S. Martins, and L. D. Flora, "Comparison of H-bridge single-phase transformerless PV string inverters," *International Conference on Industry Applications (INDUSCON), 2012 10th IEEE/IAS*, pp. 1-8, November 2012.

[24] C. Yeh and M. Manjrekar, "A reconfigurable uninterruptible power supply system for multiple power quality applications," *IEEE Trans. Power Electron*, vol. 22, pp. 1361-1372, 2007.

[25] F. Kamran and T. Habetler, "A novel on-line ups with universal filtering capabilities," *IEEE Transactions on Power Electron*, vol. 13, pp. 410-418, 1998.

[26] C. Lai and Y. Tzou, "Dsp-embedded ups controller for high performance single-phase on-line ups systems," *In Industrial Electronics, 2009. IECON 09. 35th Annual Conference of IEEE*, pp. 268173, November 2002.

[27] S. L. E. C. Y. Feng, C. Lai and Y. Tzou, "Dsp-based fully digital control of an on-line ups," *The 4th IEEE International Conf, on Power Electron, and Drive Sys*, 2001.

[28] R. B. R. C. Zhou and F. C. Lee, "Design and analysis of a hysteretic boost power factor correction circuit," *Inn Proc. IEEE PESC*, pp. 800807, 1990.

[29] S. B. Z. Nie and A. Emadi, "An on-line ups system with power factor correction and electric isolation using bifred converter," *In The 29th Annual Conf. of the IEEE. Industrial Electron. Society*, vol. 1, pp. 361366, November 2003.

[30] D. M. C. T. M. M. Jovanovic and F. C. Lee, "Reduction of voltage stress in integrated high-quality rectifier-regulators by variable-frequency control," *In Proc. IEEE APEC*, pp. 569575, 1994.

[31] P. D. Z. M. Kazerani and G. Joos, "A novel active current waveshaping technique for solid-state input power factor conditioners," *IEEE Trans. Ind. Electron*, vol. 38, pp. 7278, 1991.

[32] H. N. A. Nabae and A. Arai, "Novel sinusoidal converters with high power factor," *In Industry Applications Conference, 1994. 39th IAS Annual Meeting.* Conference Record of the 1994 IEEE, 1994.

[33] I. Soares de Freitas, C.B. Jacobina, and E.C. dos Santos, "Single-phase to single-phase full-bridge converter operating with reduced ac power in the dc-link capacitor," *IEEE Transactions on Power Electronics*, vol. 25, no. 2, pp. 272-279, February 2010.

[34] C.B. Jacobina, T.M. Oliveira, E.R.C. da Silva, "Control of the single-phase three-leg AC/AC converter," *IEEE Transactions on Industrial Electronics*, vol. 53, no. 2, pp. 467-476, April 2006.

[35] E.C. dos Santos Junior, S. Sajadian,"Energy conversion unit with optimized waveform generation," *Industry Applications Society Annual Meeting, 2013 IEEE*, pp. 1-6, October 2013.

[36] T. Liang, J. Shyu, and J. Chen, "High real output power on-line UPS system with built-in reactive power compensation," *IEEE 32nd Annual Power Electron. Specialists Conf*, vol. 3, pp. 1555-1560, June 2001

[37] M. Khoor, and M. Machmoum, "A novel single-phase reduced parts on-line UPS with power quality conditioning capability," *IEEE Power Electron. Specialists Conference*, pp. 1170-1175, June 2007.

[38] A. Kayabasi, and R. Akkaya, "The design and implementation of a microcontroller-based single phase on-line uninterrupted power supply with power factor correction," *International Conf. on Electrical and Electronics Engineering, ELECO 2009*, pp. 442-446, November 2009.

[39] S. M. Bashi, J. Jasni, and O.Y. Weng, "Voltage regulation of uninterrupted power supplies," *Student Conf. on Research and Development, SCORED 2003. Proceedings*, pp. 385-389, August 2003.

[40] J. C. Hwang, J. C. Chen, J. S. Pan, and Y. C. Huang, "Measurement method for online battery early faults precaution in uninterrupted power supply system," *Electric Power Applications, IET*, vol. 5, no. 3, pp.267-274, March 2011.

[41] I. Daut, M. Irwanto, and S. Hardi, "Photovoltaic powered uninterruptible power supply using smart relay," *Power Engineering and Optimization Conf*, pp. 453-457, June 2010.

[42] W. Zhang, D. Xu, X. Li, R. Xie, H. Li, D. Dong, C. Sun, and M. Chen, "Seamless transfer control strategy for fuel cell uninterruptible power supply system," *IEEE Transactions on Power Electronics*, vol. 28, no. 2, pp. 717-729, February 2013.

[43] I. Galkin, A. Stepanov, and P. Suskis, "Selection of power factor corrector for modular uninterruptable power supply system," *Power Electronics and Motion Control Conf*, pp. 13-21, September 2010.

[44] J. Williams, and D. Beebe, "Diode turn-on time induced failures in switching regulators," *Linear Technology*, *Application Note 122*, January 2009.

[45] R. H. Stevens, "Power flow direction definitions for metering of bidirectional power," *IEEE Transactions on Power Apparatus and Systems*, vol. PAS-102, no. 9, pp. 3018-3022, September 1983.

[46] T. L. Bourbonnais, and L. J. Lunas, "A versatile phase-angle meter for power system analysis," *IEEE Transactions on Power Apparatus and Systems*, vol. PAS-86, no. 6, pp. 734-750, June 1967.

[47] A. Reznik, M. G. Simoes, A. Al-Durra, and S. M. Muyeen, "LCL filter design and performance analysis for grid-interconnected systems," *IEEE Transactions on Industry Applications*, vol. 50, no. 2, pp. 1225-1232, March 2014.

[48] A. Reznik, M. G. Simoes, A. Al-Durra, and S. M. Muyeen, "LCL filter design and performance analysis for small wind turbine systems," *Power Electronics and Machines in Wind Applications*, 2012 *IEEE*, pp.1-7, July 2012.

[49] F. Bouchafaa, D. Beriber, and M. S. Boucherit, "Modeling and control of a gird connected PV generation system," *Control & Automation (MED),2010 18th Mediterranean Conference*, pp.315-320, June 2010.

[50] M. Liserre, F. Blaabjerg, S. Hansen, "Design and control of an LCL-filter based three-phase active rectifier," *Industry Applications Conference Thirty-Sixth IAS Annual Meeting. Conference Record of the* 2001 *IEEE*, vol. 1, pp. 299-307, September 2001.

[51] T. Yi, C. L. Poh, W. Peng, H. C. Fook, G. Feng, and F. Blaabjerg, "Generalized design of high performance shunt active power filter with output LCL filter," *IEEE Transactions on Industrial Electronics*, vol. 59, no. 3, pp. 1443-1452, March 2012.

[52] M. Raoufi,and M. T. Lamchich, "Average current mode control of a voltage source inverter connected to the grid: application to different filter cells," *Journal of Electrical Engineering*, vol. 55, no. 3-4, pg. 77-82, 2004.

[53] E.C. dos Santos Junior, S. Sajadian, "Energy conversion unit with optimized waveform generation," *Industry Applications Society Annual Meeting, 2013 IEEE*, pg. 1-6, October 2013.

[54] Grid-tie inverter. Digital image. *EcoDirect*. [Online]. Available: http://www.ecodirect.com/Grid-Tie-Inverter-s/38.htm (Last day accessed: November 11, 2014.)

[55] "DIY PV system," *Deciding on the type of PV system to install*. [Online]. Available: http://www.builditsolar.com/Projects/PV/EnphasePV/TypeOfSystem.htm (Last day accessed: November 03, 2014.)

[56] Typical block diagram of a grid-tie PV system. Digital image. UIC Grid Tied PV Systems. [Online]. Available: http://www.unityintegration.com/vert_grid.html (Last day accessed: November 06, 2014.)

[57] O. Smith, "Enphase M250." Digital image. *Business Wire*. 17 June 2014. [Online]. Available: http://www.businesswire.com/news/home/20140617006687/en/Enphase-Energy-Launches-World%E2%80%99s-Fourth-Generation-Microinverter-System%20-%20.VGACbvnF_pU#.VH-7AjHF_pU (Last day accessed: November 06, 2014.)

[58] Solar Bridge. Digital image. TGALsolar. [Online]. Available: http://tgalsolar.com/products/solar-electricity/grid-connected/australian-made-system/enecsys-micro-inverter/ (Last day accessed: November 06, 2014.)

[59] Micro-inverter. Digital image. Get Micro-inverter. 25 August 2014. [Online]. Available: http://mesapreservationfoundation.org/get-micro-inverter/ (Last day accessed: November 06, 2014.)

[60] Involar M250. Digital image. Miniwindshop. [Online]. Available: http://ecopen.homelinux.net/miniwindshopQB/online-shop/solar-pv/involar-m250-microinverter/ (Last day accessed: December 03, 2014.)

[61] SMA inverter. Digital image. Wholesale Solar. [Online]. Available: http://www.wholesalesolar.com/products.folder/inverter-folder/SMA-Sunny-Boy-240-US.html (Last day accessed: December 03, 2014.)

[62] H. Hyder, "Piping Technology & Products." Snubbers: A General Overview. 02 December. 2010. [Online]. Available: http://www.pipingtech.com/technical/articles/snubbers-hydraulic-mechanical.htm (Last day accessed: November 06, 2014.)

[63] A. E. Fitzgerald, C. Kingsley Jr, and S. D. Umans, "Synchronous Machines." Electric Machinery. 6th ed. New York: E. A. Jones, 2005. pg. 266-275. Print.